Chapter 4: Production of Tyrosine Kinase Inhibitors from *Streptomyces clavuligerus*

4.1 Introduction

The genus *Streptomyces* is a member of the phylum Actinomycetota, displaying a distinct characteristic of having a high GC content (70%) within its genetic material (Procópio et al., 2012). It is a filamentous form, aerobic, gram-positive, saprophytic, and soil-dwelling bacteria that possess the potential to synthesize a vast range of secondary metabolites, including antibiotics (Kapadia et al., 2007; Watve et al., 2001). *Streptomyces* is considered a vital source in drug discovery, as it synthesizes a substantial proportion (80%) of antibiotics currently used to combat various diseases (Běhal, 2000). Some of the most well-known antibiotics produced by *Streptomyces* include streptomycin, tetracycline, and erythromycin. Additionally, *Streptomyces* species produced other bioactive compounds, such as immunosuppressants, anticancer agents, protein kinase inhibitors, apoptosis inducers, and caspase-3 activators (Chin et al., 2006; Sun et al., 2017). An example of an anticancer drug synthesized by *Streptomyces* is daunorubicin, which is a chemotherapy drug used to treat various types of leukemia and other cancers (Hutchinson, 1997).

Streptomyces clavuligerus is a soil bacterium of the phylum Actinobacteria that produces aerial, dark greyish mycelium, which comprises sympodial, branched hyphae and spores (Higgens & Kastner, 1971; Saini et al., 2023a). It generates β-lactam antibiotics: clavulanic acid, cephamycin C, penicillin N, O-carbamoyl derivative deacetylcephalosporin C, and deacetoxycephalosporin C (Nabais & da Fonseca, 1995). It also forms non-β-lactam secondary metabolites, holomycin, and complex MM 19290 (Baggaley et al., 1997). Clavulanic acid is a novel β- lactamase inhibitor (broad-spectrum antibiotic) effective against gram-positive and gram-negative bacteria. Its salt and ester can enhance the impact of β-lactam antibiotics against bacteria that produce β-lactamase (Reading & Cole, 1977; Saudagar et al.,

2008). It also engenders a proteinaceous beta-lactamase inhibitor, BLIP, structurally unrelated to clavulanic acid (Doran et al., 1990b). It also retains the ability to produce kinase and phosphatase inhibitors, which can be lead molecules in the target-based treatment of diseases (Běhal, 2000). The genus *Streptomyces* possesses both eukaryotic signalling systems and prokaryotic two-component regulatory systems, making it a promising candidate for developing an assay for screening kinase inhibitors in eukaryotic signalling pathways. *Streptomyces 85E* has been identified as a suitable strain for testing kinase inhibitors using agar diffusion methods due to its growth and development characteristics on solid media and its ability to reveal the cytotoxicity of tested inhibitors (Watersa et al., 2002). The *Streptomyces 85E* assay exhibits distinct phenotypes that can be utilized to deduce the persistence of eukaryotic protein kinase inhibitors (Shanbhag et al., 2015a).

This chapter aimed to produce bioactive compounds from *Streptomyces clavuligerus* by submerged fermentation and identification of secondary metabolites present in the aqueous and organic crude extracts of *Streptomyces clavuligerus* by High-Resolution Liquid Chromatography-Mass Spectrometry technique. Additionally, eukaryotic protein kinase inhibitory potential and *invitro* cytotoxicity study against MCF-7 (Human breast cancer), Hop-62 (Lung cancer), SiHa (cervical cancer), and PC-3 (prostate cancer) cell lines of *Streptomyces clavuligerus* extract were conducted to evaluate the anticancer potential of *Streptomyces clavuligerus.* Furthermore, the inhibitory potential of identifying secondary metabolites of *Streptomyces clavuligerus* against several Receptor Tyrosine Kinases (RTKs) such as Insulin Growth Factor Receptor (IGFR), Hepatocyte Growth Factor Receptor (HGFR), Fibroblast Growth Factor Receptor (FGFR) family, Vascular Endothelial Growth Factor Receptor (VEGFR) family, Platelet-Derived Growth Factor Receptor (PDGFR) family, and Epidermal Growth Factor Receptor (EGFR) family

was employed by *insilico* approach including molecular docking, dynamic simulation, and MM/GBSA analysis for pharmacological drug discovery and cancer therapy.

4.2 Materials and Methods

4.2.1 Cancer Cell Line and *Streptomyces 85E* strain

MCF-7 (Human breast cancer), Hop-62 (Lung cancer), SiHa (cervical cancer), and PC-3 (prostate cancer) cell lines were acquired from the National Centre for Cell Science (NCCS) Pune, India; *Streptomyces 85E* (ATCC 55824) was obtained as a gift sample from Prof. (Dr.) Julian Davies and Mr. Ivan Villanueva.

4.2.2 Procurement and maintenance of *Streptomyces clavuligerus*

Streptomyces clavuligerus was obtained from the Microbial Type Culture Collection (MTCC), Institute of Microbial Technology, Chandigarh, India, with **MTCC No. 1142.** The **s**trains were cultured and maintained on ISP4 agar medium containing (wt/v): ammonium sulfate (0.2%), di-potassium hydrogen phosphate (0.1%), magnesium sulfate (0.1%), sodium chloride (0.1%), calcium carbonate (0.2%), soluble starch (1.0%), agar (2%) and a Trace Salt Solution (TSS) consisting of ferrous sulfate (0.1%), zinc sulfate (0.2%), copper sulfate (0.7%) and manganous chloride (0.8%). 1 mL of TSS was dissolved in 1 L of media, and the pH was adjusted to 7.0. The isolated and marked strains were periodically re-cultured on ISP-4 agar medium to ensure their growth and maintenance (Kobayashi et al., 1994).

4.2.3 Colony separation and microscopic examination

The isolation and examination of *Streptomyces clavuligerus* begins with streaking a sample onto an ISP-4 agar medium, sterilized at 121°C for 15 minutes, and incubated at 30°C for 5-7 days to allow colony growth. Well-separated colonies are selected based on morphology and subcultured onto fresh agar plates, which are incubated again to confirm purity.

For microscopic examination, a smear of the isolated colony is prepared on a glass slide to observe the characteristic filamentous structures of *Streptomyces clavuligerus*.

4.2.4 Fermentation-based production of bioactive compounds

Media: The seed media was composed of glucose (1.5%), peptone (0.75%), yeast extract (0.75%), corn steep liquor (0.5%), sodium chloride (0.5%), and calcium carbonate (0.2%). The production media was composed of glucose (5%), yeast extract (1.1%), calcium carbonate (0.5%), peptone (0.4%), beef extract (0.4%), and sodium chloride (0.25%) (Shanbhag et al., 2015a).

Fermentation Condition: The inoculum was harvested from *Streptomyces clavuligerus* ISP-4 agar media plate after 72 hours, mixed with 50 mL of seed media, and incubated at 30°C under 200 RPM for three days. Afterward, the batch fermentation was conducted in a 500 mL flask containing 100 mL of autoclaved production media by inoculating it with 3 mL of seed media and incubating it at 30°C with 200 RPM for three days.

` Microbial Growth and Metabolite Production

To measure biomass growth and metabolite production, *Streptomyces clavuligerus* was fermented in growth media at 30°C for three days. Samples were collected every 3 hours over a period of 72 hours, and biomass measurement was taken to calculate dry cell mass (g/L). To quantify metabolite production of the total red anthracycline, the absorbance of the filtrate was measured at 498 nm using a spectrophotometer. Subsequently, the absorbance values were calculated in (g/L) utilizing a standard curve generated from pure epirubicin (Thakur et al., 2009).

4.2.6 Downstream process of secondary metabolites

The downstream process was conducted through a two-phase solvent extraction technique after the completion of the fermentation step (Madduri, Kennedy, Rivola, Inventi-Solari, Filippini,

Zanuso, et al., 1998). The broth was divided into two halves and subjected to aqueous and organic extraction.

Aqueous extraction: One part of the broth was centrifuged for 20 minutes at 6000 rpm and 4°C. Most of the supernatant was collected, and the remaining supernatant with cell debris or pellet was subjected to sonication in 10-minute cycles with 5-minute breaks for 30 minutes. The mixture was centrifuged to extract intracellular components, and the resultant supernatant was collected. All the supernatants were amalgamated, subjected to lyophilization, and preserved at a temperature of -20°C for future use.

Organic extraction: The other part of the broth underwent sonication, and then it was combined with twice its volume of a solvent mixture with a 1:6 v/v ratio of chloroform to isopropanol. This step resulted in a final mixture of one part broth to two parts solvent, with a 1:2 v/v ratio. The mixture was incubated for 24 hours at 45±1°C and agitated at 200 rpm. The organic phase was separated from the broth through a conical separating funnel and subjected to vacuum evaporation to yield a crude extract, which was then stored at -20°C.

4.2.7 Protein kinase inhibitory assay (*Streptomyces 85E* assay)

The organic extract of *Streptomyces clavuligerus* was subjected to a protein kinase inhibitory study with Streptomyces 85E and used as the model strain. The frozen organic extract was thawed, mixed, and reconstituted in DMSO to a 20 mg/mL concentration. The solution was sterilized through filtration using a sterile 0.45 µm nylon syringe filter, and the filtrate was stored at -20°C for immediate use. *Streptomyces 85E* (ATCC 55824) was cultured in Luria-Bertani broth at 30°C and 180 rpm for three days. It was inoculated utilizing the spread plate technique on the ISP-4 agar media plate. A well (6 mm diameter) was made in the plates, and a 160 µL sample was dispensed into the well. 100% pure DMSO was taken as a negative control, while the positive control was the widely known

tyrosine kinase inhibitor doxorubicin. The plates were incubated at 30 °C for three days and subsequently examined for evidence of protein kinase inhibitory potential (Watersa et al., 2002).

4.2.8 Free radical scavenging activity

The free radical scavenging activity of organic and aqueous extracts of *Streptomyces clavuligerus* was evaluated through DPPH assay using the methodology described by Kamble et al., with minor modifications (Kamble et al., 2018). The assay assesses the potential of the extract to reduce the free radicals through one-electron reduction. Briefly, different concentrations (1 to 40 µg/mL) of the *Streptomyces clavuligerus* extract were made with a total volume of 3 mL using methanol. In each test tube, 1 mL of a 0.1 mM DPPH solution was added and shaken quickly. The test tubes were left at room temperature, in the dark, for 30 minutes. L-ascorbic acid was used as a positive control. The absorbance was measured using spectrophotometry at a wavelength of 517 nm in order to estimate the free radical reduction. The radical scavenging activity of extracts was depicted as the inhibition percentage and calculated using the following formula:

$$\text{Inhibition percentage} = [(A_0 - A_s) \div A_0] \times 100$$

Where A_o is the absorbance control, and A_s is the absorbance of the extracts, the percentage scavenging activity against the extract concentration was plotted to represent the results, and the IC_{50} value was calculated from the graph.

4.2.9 Cytotoxicity Assay

The cytotoxic potential of the organic microbial crude extract of *Streptomyces clavuligerus* was conducted against MCF-7 (Human breast cancer), Hop-62 (Lung cancer), SiHa (cervical cancer), and PC-3 (prostate cancer) cell lines through the MTT assay. All the cancer cell lines were cultivated in T-25 flasks, detached using trypsin, and collected in a 5 mL centrifuge tube. Subsequently, centrifugation was carried out at 300

x g to generate a cell pellet. The cell count was then adjusted using DMEM-HG medium to achieve approximately 10,000 cells suspended in 200 µL. Then, 200 µL of the cell suspension was added to each well of a 96-well microtiter plate. The plate was then placed in an incubator at 37°C with 5% CO2 for 24 hours (Bhatnagar et al., 2022; Kumari, Saini, & Mishra, 2023a; M. H. Nguyen et al., 2024; Van Meerloo et al., 2011).

Following the incubation period, the used medium was extracted, and 200 µL of different concentrations of extracts (10 to 80 µg/mL) were introduced into their respective wells. The plate was then placed in an incubator at 37°C in a 5% CO2 environment for 24 hours. Following this incubation period, the medium containing the drug was removed, and 200 µL of medium containing 10% MTT reagent was added to each well, resulting in a final concentration of 0.5 mg/mL. The plate was then placed in an incubator at 37°C with 5% CO2 for 3 hours. After this incubation period, the culture medium was aspirated without disturbing the crystals. Next, 100 µL of DMSO was introduced, and the plate was gently agitated using a gyratory shaker to dissolve the resulting formazan crystals. Absorbance measurements were then taken using a microplate reader at 570 nm and 630 nm wavelengths (Patel et al., 2013; Van Tonder et al., 2015). The percentage of growth inhibition was computed after subtracting the background and blank readings. From the dose-response curve, the concentration of crude extract required to inhibit 50% of cell growth (IC_{50}) was determined (Vijayarathna & Sasidharan, 2012).

The percentage of growth inhibition was determined using the following formula:

$$\%\ Growth\ inhibition\ =\ [Ti\ /\ C]\ \times 100\%$$

$$[(Growth\ in\ the\ presence\ of\ drug\ at\ various\ concentration\ levels)$$

$$/\ Control\ growth]\ \times\ 100\%.$$

Where Ti is the growth in the presence of drugs at various concentration levels, and C is the controlled growth or growth of the cell line without extract.

4.2.10 HR-LCMS for Identification of Secondary Metabolites

The presence of metabolites in the organic and aqueous extract of the *Streptomyces clavuligerus* was determined by applying the high-resolution liquid chromatography-mass spectrometry (HRLCMS) technique (Holčapek et al., 2012; Kumari, Saini, & Mishra, 2023b). The appropriate amount of sample was combined with acetonitrile and analyzed using a Thermo Fischer Scientific Q-Exactive Plus Biopharma-High Resolution Orbitrap Liquid Chromatograph Mass Spectrometer (HR-LCMS) instrument consisting of a Hypersil GOLD C18 100 x 2.1 mm-3-micron column, a HiP Sampler (model: G4226A), a binary pump (model: G4220B), a Column compartment (model: G1316C) and a Diode-Array Detector (model: G4212B) from Agilent Technologies. The chromatography system was conditioned with 5% Acetonitrile, and the analysis was conducted with a flow rate of 0.3 mL/min for 30 minutes using a 5.00 µL injection volume with 100% Acetonitrile. The mass spectrometer analysis was performed on the compounds using a Q-ToF (model: G6550A) instrument with a sheath gas temperature of 300°C, a nebulizer pressure of 35 psi, a gas flow rate of 13 L/min, and a gas temperature of 250°C**.**

4.2.11 Molecular Docking of metabolites with RTKs.

The formation of "bald" colonies or cloudy zones observed in *Streptomyces 85E* is associated with the secondary metabolites possessing eukaryotic protein kinases inhibitory potential. An in-silico approach was employed to gain a brief understanding of the potential metabolites of *Streptomyces clavuligerus* that interact with different RTKs. The structure of various RTKs with mutations was obtained from the PDB database (www.rcsb.org), including VEGFR-2 (3U6J), PDGFR-A (6JOI), FGFR-4 (5XFJ), ALK (2YFX), AXL (7DXL), IR (4IBM), and EGFR (5HG8). The structure of protein kinase was optimized through the Protein Preparation Wizard within the Schrödinger software package. Their structural imperfections were rectified using the EPIK module. Water

molecules were removed from the receptors and optimized to a stable state with the help of the OPLS4 Force field (Leslie et al., 2021).

The secondary metabolites of *Streptomyces clavuligerus* obtained from the HR-LCMS analysis were depicted using the Marvin sketch 21.12 software from ChemAxon (https://www.chemaxon.com) and were stored in the mol2 format. The LigPrep module of Schrödinger (Schrödinger Release 2022-2) was used to prepare the ligands and OPLS4 force field to neutralize their ionization state and other parameters as default (S. Kumar et al., 2018). The Receptor Grid Generator Module generated a grid for each protein, which was the receptor input for molecular docking. It involved the selection of a co-crystallized ligand of the loaded protein and the subsequent creation of a grid box encompassing the ligand binding site with default spacing. Molecular docking was carried out using the Glide component of the Schrodinger suite, with each protein kinase receptor being docked against a prepared ligand library of *Streptomyces clavuligerus.* Docking was conducted at the Extra Precision (XP) level, including ten poses per ligand in post-docking minimization, and keeping another parameter intact. The results were analysed based on the Glide score (K. Banerjee et al., 2011).

4.2.12 Molecular Dynamics Simulation

The molecular dynamics simulation was performed for standard ligands and selected docked protein-ligand complexes through the Desmond module within the Schrödinger Suite software package. A neutralized TIP3P water model was generated within an orthorhombic solvation box, and counter ions were added to reach a neutral charge. (Ahmad, 2022). The system was then brought to a 0.15 M NaCl concentration and subjected to 1000 ps minimization with the OPLS system forcefield. (Chandar et al., 2019; Kalra et al., 2021). The system was equilibrated through a relaxation protocol utilizing default settings, followed by 160 ps of combined NVT and NPT simulation. After this, MD was conducted

for 200 ns with a 0.25 ns time interval, giving a 2000-frame trajectory, and OPLS force field parameters were employed throughout the simulations (Sigalapalli et al., 2020). After the completion of the molecular dynamics simulation, various metrics were calculated and analyzed, including RMSD, RMSF, SASA, and Rg. The molecular interaction of ligands with receptors was also assessed.

The binding free energy of the protein-ligand complexes was determined using the molecular mechanics generalized Born surface area (MM-GBSA) method, using the following equation to express the binding free energy.

$$\Delta Gbinding = \Delta Gcomplex - [\Delta Gprotein + \Delta Gligand]$$

ΔGbinding represents the binding free energy of the protein-ligand complexes, while ΔGprotein and ΔGligand represent the energies of the protein and ligand, respectively. The Prime module was utilized to perform the MM-GBSA calculation, and the last 20 ns of the simulation trajectory was employed as input (Nada et al., 2022).

Further, per-residue decomposition analysis was performed to evaluate the energetic contributions of individual amino acids in inhibitor binding. This analysis was conducted through the prime module using the "breakdown_MMGBSA_by_residue" script, which deconstructs the binding energy of each complex into its component parts (Agarwal et al., 2022).

4.3 Results and Discussions

4.3.1 Colony separation and microscopic examination

The isolation procedures successfully produced well-separated colonies of *Streptomyces clavuligerus* on ISP4 agar medium. The microscopic result is represented in Figure 4**.1.** which revealed a complex, aerial dark greyish mycelium structure with branched hyphae of *Streptomyces clavuligerus* (Bascarán et al., 1990; Nithya et al., 2017).

4.3.2 Microbial Growth and Metabolite Production

The growth and metabolite production curves for *S. clavuligerus* depicted biomass accumulation and secondary metabolite production over a 72-hour period, as shown in Figure 4.2. Biomass growth was measured by determining the dry cell mass at 3-hour intervals, while metabolite production was assessed spectrophotometrically at 498 nm. The biomass growth curve exhibited a rapid increase in cell mass, reaching 4 g/L at 30 hours. After this point, the growth rate decelerated, with biomass gradually rising to 7 g/L by the 72-hour mark. This trend represents a typical bacterial growth pattern, with an initial log phase followed by a stationary phase, indicating that optimal growth for *S. clavuligerus* occurs within the first 24 hours (Ghaly et al., 2003).

Metabolite production began to increase after 24 hours, sharply rising to 1.4 g/L by the end of the 72-hour period, after which the production rate plateaued. After 24 hours, both biomass and metabolite production increased, though the rate of biomass growth slowed. This pattern indicates an initial lag phase with minimal metabolite production, followed by simultaneous growth and production (Williams et al., 2012).

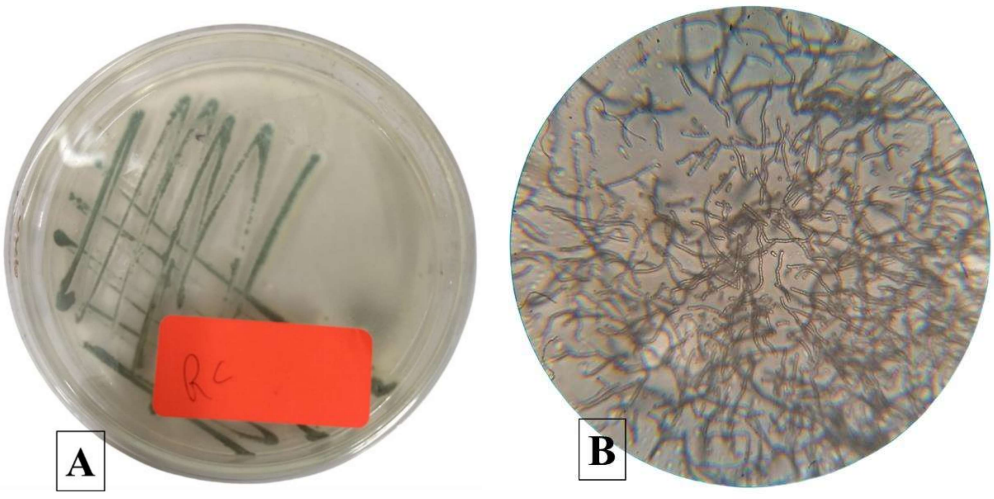

Figure 4.1: Plate A represents the cultured plate of *Streptomyces clavuligerus* (MTCC 1142), and plate B is the microscopic image of *Streptomyces clavuligerus* at 100X.

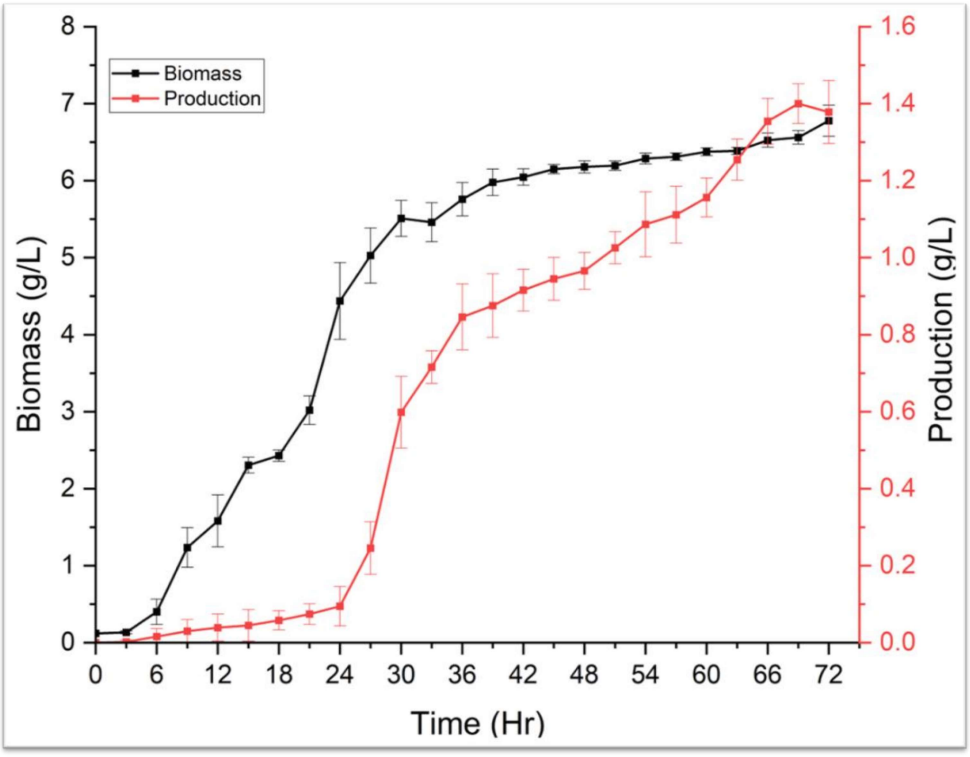

Figure 4.2: The growth curve (black line) and metabolite production curves (red line) for *S. clavuligerus* represent the biomass accumulation and secondary metabolite production over a 72-hour period.

4.3.3 *Streptomyces 85E* assay (Kinase inhibition assay)

The protein kinase inhibitory potential of *Streptomyces clavuligerus* crude extracts was evaluated through the *Streptomyces 85E* assay by assessing the growth pattern of *Streptomyces 85E*. The absence of any zone in the test plates indicates the lack of PKIs in the sample. A whitish bald zone or hazy zone in the plates signifies the presence of PKIs, while the presence of a clear zone signifies the complete growth inhibition of *the Streptomyces 85E* strain, which could be attributed to the presence of antimicrobial activity.

The results of a kinase inhibition assay exhibited intense inhibitory activity against protein kinases, resulting in the formation of a bald or hazy zone on the assay plate with a diameter of approximately 18 mm, as presented in **Figure 4.3. A**. Doxorubicin was used as a positive control, indicating the presence of a thin, hazy line along the edge of the

clear zone, with a diameter of 0.66 mm, indicating the presence of protein kinase inhibitory potential, as depicted in **Figure 4.3. B.** Dimethyl sulfoxide (DMSO) was used as a negative control (**Figure 4.3. C.).** These findings suggest that *Streptomyces clavuligerus* could be a potential source of novel bioactive compounds for further exploration in drug discovery and development against cancer.

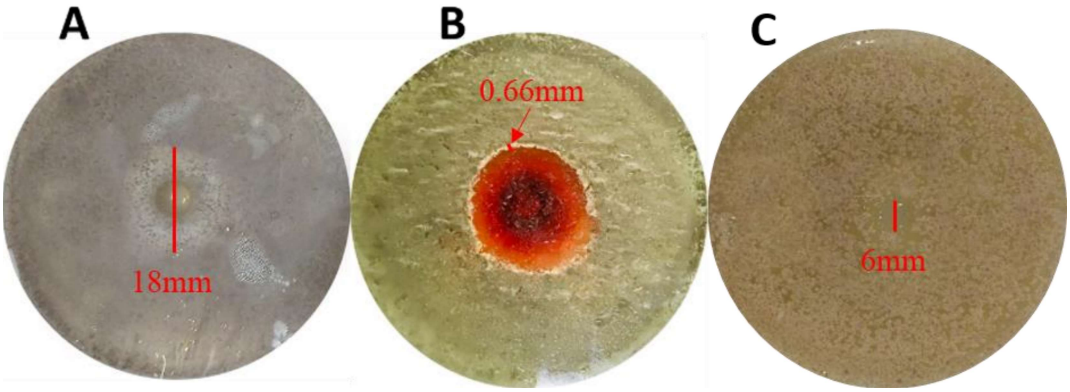

Figure 4.3: Plate A showed 18 mm diameter whitish hazy zones due to *Streptomyces clavuligerus extracts,* while plate B (positive control) showed a 0.66 mm diameter thin and hazy line from doxorubicin. The negative control in plate C, represented by DMSO, did not show any zone formation. Whitish hazy zones suggest the existence of Protein Kinase Inhibitors, and clear zones denote complete bacterial inhibition.

4.3.4 The free radical scavenging activity

The free radical scavenging activity of different concentrations of extracts derived from *Streptomyces clavuligerus* extract was illustrated in Figure 4.4. Notably, the organic extract of *Streptomyces clavuligerus* exhibited a more robust free radical scavenging capacity, with an IC_{50} value of 28.90 ± 0.24 µg/mL, in contrast to the aqueous extract, which displayed an IC_{50} value of 74.30 ± 1.13 µg/mL. However, it was found that the efficacy of the organic extract was lower than that of the standard drug ascorbic acid, which had an IC_{50} value of 14.38 ± 0.14 µg/mL. These results indicate that, at concentrations up to 5 µg/mL, the inhibitory potential of both the aqueous and organic extracts were comparable. Beyond this concentration threshold, the organic extract demonstrated increasingly superior inhibitory potential. At a higher concentration of 40

µg/mL, the organic extract exhibited a maximum inhibition percentage of 61 ± 1.04%, while the aqueous extract reached a maximum inhibition percentage of 30 ± 0.85%. In contrast, the standard drug, ascorbic acid, displayed the highest inhibition percentage of 98 ± 0.24%, as depicted in Figure 4.4.

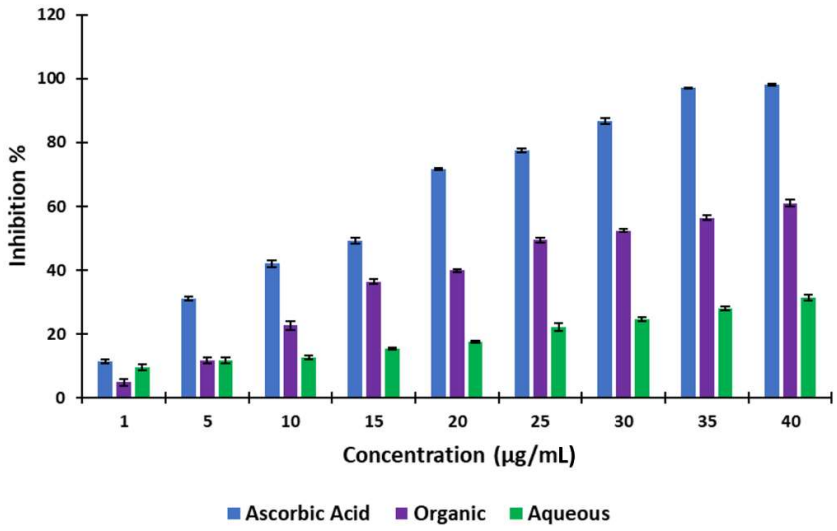

Figure 4.4: The free radical scavenging activity of various concentrations of organic and aqueous extract of *Streptomyces clavuligerus*

4.3.5 Cytotoxicity analysis

The cytotoxicity activity of the microbial extracts of *Streptomyces clavuligerus* was evaluated using the MTT assay to determine their half-maximal inhibitory concentration (IC_{50}) values. The IC_{50} value of the extract against MCF-7, Hop-62, SiHa, and PC-3 cell lines was 128.93±3.1 µg/mL, 464.48±9.2 µg/mL, 278.15±4.77 µg/mL, and 353.14±7.3 µg/mL, respectively. The findings showed that the extract's IC_{50} value was most minimal for the MCF-7 cell line, then for the SiHa cell line, indicating strong potential to inhibit the growth of human breast cancer and human cervical cancer cell lines. The growth percentage of these cell lines with different concentrations of the extract is presented in Figure 4.5. This result underscores the importance of further investigation of the extract to identify and isolate the specific active compounds and determine their mechanisms of

action. Ultimately, this information could lead to the development of new and more effective treatments for cancer.

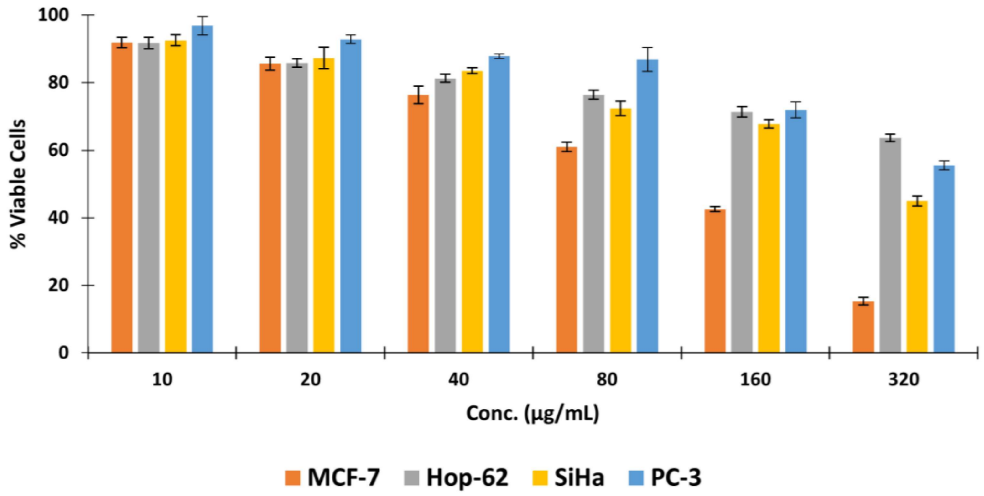

Figure 4.5: Percentage growth of MCF-7, Hop-62, SiHa, and PC-3 cancerous cell lines (cultured at 37 °C temperature, 5:95 of CO2: air composition, and 100% RH for 24hr) with varying concentrations of the organic *Streptomyces clavuligerus's* microbial extracts

4.3.6 HR-LCMS analysis

The organic extract of *Streptomyces clavuligerus* was subjected to HR-LCMS analysis to determine its chemical composition, having an abundance score above 1000. The chromatography technique facilitated the presence of the secondary metabolites based on their retention time, the mass-to-charge ratio (m/z), reference databases, and proposed chemical structures. HRLCMS chromatogram of aqueous and organic extract of *Streptomyces clavuligerus* is represented in Figure 4.6. The mass-to-charge ratios (m/z) for the secondary metabolites present in the aqueous extract ranged from 161 to 747, while for the organic extract, they varied between 107 and 741.

The observed m/z values suggest the presence of diverse secondary metabolites with different molecular sizes and charges in both extracts. This information could be helpful for further analyzing and identifying these metabolites using methods such as mass

spectrometry or chromatography. The identified secondary metabolites from the aqueous and organic extracts of *Streptomyces clavuligerus* are documented in Tables 4.1 and 4.2.

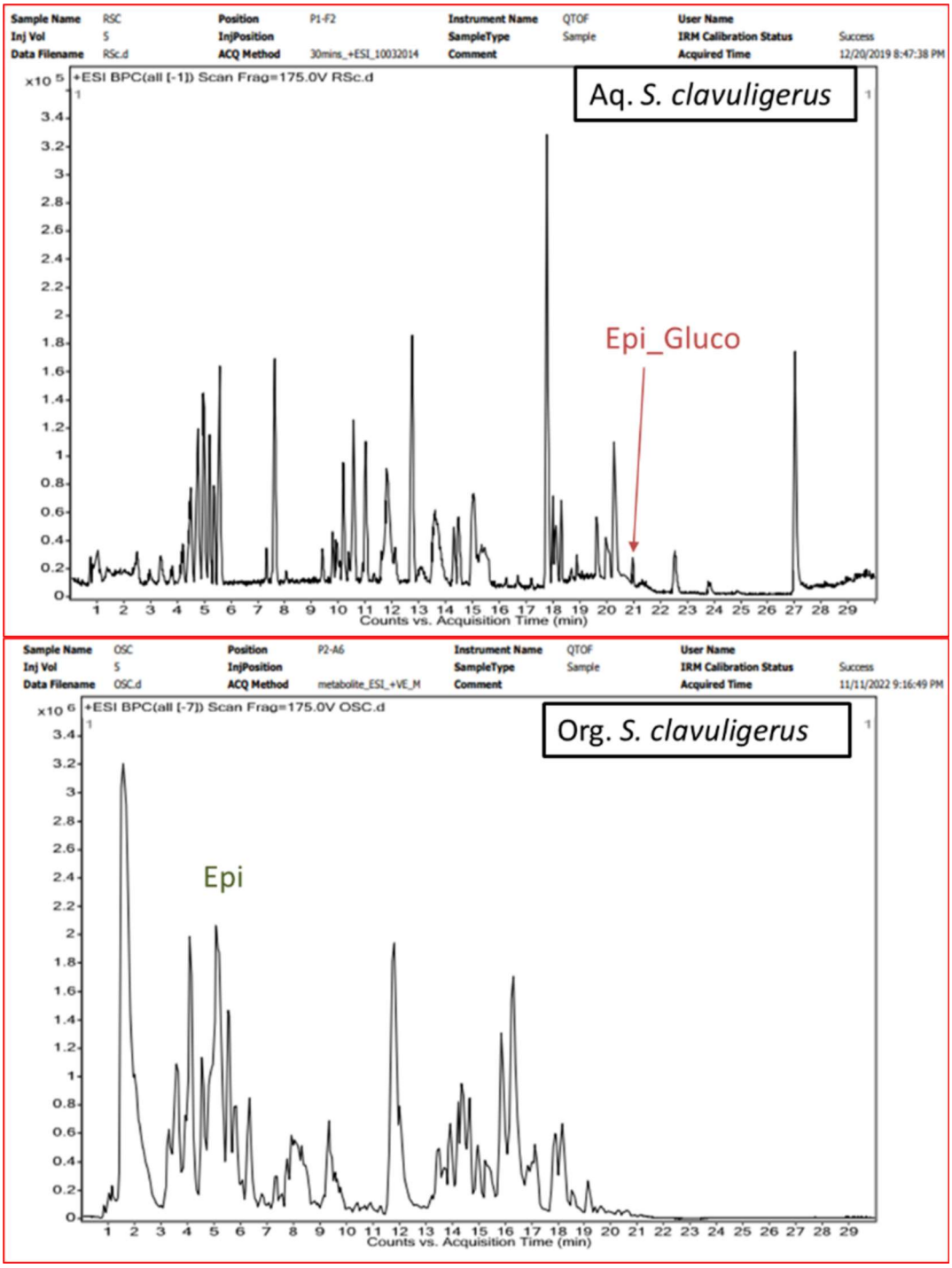

Figure 4.6: HRLCMS chromatogram of aqueous and organic extract of *Streptomyces clavuligerus* showing a great resolution peak.

Table 4.1: Secondary metabolites identified by the HR-LCMS in an aqueous extract of *Streptomyces clavuligerus*.

Aqueous				
RT	**Name**	**Mass**	**Formula**	**[m/z]**
0.186	Dimethylallyl pyrophosphate	246.00	$C_5 H_{12} O_7 P_2$	250.9813
0.75	Norcotinine	162.08	$C_9 H_{10} N_2 O$	185.0675
0.927	14-pentadecynoic acid	238.19	$C_{15} H_{26} O_2$	243.1713
0.98	Monotropein	390.12	$C_{16} H_{22} O_{11}$	395.1011
1.069	4-(2-hydroxy-3-isopropyl-aminopropyl)benzoic acid	253.13	$C_{13} H_{19} N O_4$	258.1104
1.335	Propanoic acid, 2-hydroxy-3- [(4-hydroxy-1-naphthalenyl)oxy]-	248.07	$C_{13} H_{12} O_5$	231.0662
1.399	Methazolamide	236.00	$C_5 H_8 N_4 O_3 S_2$	237.0091
1.857	sebacic acid	202.12	$C_{10} H_{18} O_4$	207.1
3.43	Dodecaprenyl phosphate- galacturonic acid	614.33	$C_{31} H_{51} O_{10} P$	321.1471
4.148	dibucaine	343.23	$C_{20} H_{29} N_3 O_2$	344.2333
4.486	Paramethasone	392.20	$C_{22} H_{29} F O_5$	393.2059
4.693	flurandrenolide	436.23	$C_{24} H_{33} F O_6$	437.2338
4.761	Gentamicin C1a	449.29	$C_{19} H_{39} N_5 O_7$	432.2864
5.142	GPEtn(10:0/11:0)[U]	537.34	$C_{26} H_{52} N O_8 P$	520.3387
5.344	(6R)-vitamin D3 6,19-(4- phenyl-1,2,4-triazoline-3,5- dione) adduct / (6R)-cholecalciferol 6,19-(4-phe	559.38	$C_{35} H_{49} N_3 O_3$	564.3657
5.353	Presqualene diphosphate	586.32	$C_{30} H_{52} O_7 P_2$	569.3201
5.506	Panaxydol chlorohydrine	296.15	$C_{17} H_{25} Cl O_2$	279.1493
5.548	1,4-Dihydroxytacrine	230.11	$C_{13} H_{14} N_2 O_2$	213.104
7.304	3-[(4-Carboxy-4- methylpentyl)oxy]-4-methylbenzoic acid (Gemfibrozil M3)	280.13	$C_{15} H_{20} O_5$	285.107
7.534	methyl 9,12-dihydroxy-13-oxo- 10-octadecenoate	342.24	$C_{19} H_{34} O_5$	325.2341
7.61	12-nitro-9Z,12Z- octadecadienoic acid	325.23	$C_{18} H_{31} N O_4$	308.2283
7.659	Naringenin	272.07	$C_{15} H_{12} O_5$	255.0654
9.764	C16 Sphinganine	273.27	$C_{16} H_{35} N O_2$	274.2743
9.91	Oxybutynin	357.23	$C_{22} H_{31} N O_3$	358.2343
10.154	Heteropeucenin, methyl ether	274.12	$C_{16} H_{18} O_4$	279.0999
10.355	Methyl jasmonate	224.14	$C_{13} H_{20} O_3$	225.1495
10.884	5beta-Cholan-24-oic Acid	360.31	$C_{24} H_{40} O_2$	343.3016
11.332	Anandamide (22:6, n-3)	371.29	$C_{24} H_{37} N O_2$	376.2662
11.604	Metaproterenol	211.12	$C_{11} H_{17} N O_3$	194.1203
11.674	Esmolol	295.18	$C_{16} H_{25} N O_4$	300.1576
11.982	7alpha- (Thiomethyl)spironolactone sulfoxide	404.20	$C_{23} H_{32} O_4 S$	387.1985

12.81	Metaproterenol 3-O-sulfate	291.08	C_{11} H_{17} N O_6 S	314.0705
13.742	Methyl 7- Desoxypurpurogallin-7-Carboxylate Trimethyl Ether	304.10	C_{16} H_{16} O_6	327.0846
14.273	Dihydrolevobunolol	293.20	C_{17} H_{27} N O_3	294.2049
14.35	6-Hydroxynicotine (R)	178.11	C_{10} H_{14} N_2 O	161.1046
15.071	Lactone of PGF-MUM	296.16	C_{16} H_{24} O_5	279.1587
15.222	GPEtn(13:0/13:0)	607.43	C_{31} H_{62} N O_8 P	590.4232
15.534	2-tetracosanamidoethanesulfonic acid	475.36	C_{26} H_{53} N O_4 S	458.3545
15.574	13R-hydroxy-9E,11Z- octadecadienoic acid	296.24	C_{18} H_{32} O_3	279.2318
16.664	Crustecdysone	480.31	C_{27} H_{44} O_7	485.2951
17.971	SM(d18:1/16:0)	703.57	C_{39} H_{80} N_2 O_6 P	686.5713
18.148	N-(2-hydroxyethyl)palmitamide	299.28	C_{18} H_{37} N O_2	282.2786
18.279	SM(d18:0/18:0)	733.62	C_{41} H_{86} N_2 O_6 P	738.6011
19.597	SM(d18:1/20:0)	759.64	C_{43} H_{88} N_2 O_6 P	742.6355
19.63	1-docosanoyl-2- (4Z,7Z,10Z,13Z,16Z,19Z-docosahexaenoyl)-sn-glycerol	724.60	C_{47} H_{80} O_5	747.5894
20.049	N-Palmitoyl-L-serine phosphoric acid	423.24	C_{19} H_{38} N O_7 P	406.24
20.384	DL-PDMP	390.28	C_{23} H_{38} N_2 O_3	391.2911
20.965	Epirubicin glucuronide	719.21	C_{33} H_{37} N O_{17}	702.2101
27.02	Ergoline-8-methanol, 10- methoxy-1,6-dimethyl-	300.19	C_{18} H_{24} N_2 O_2	305.1635
27.112	Prometon	225.16	C_{10} H_{19} N_5 O	230.1411

Table 4.2: Secondary metabolites identified by the HR-LCMS in the organic extract of *Streptomyces clavuligerus*.

Organic				
RT	**Name**	**Mass**	**Formula**	**[m/z]**
1.146	(3beta,22R,23R,24S)-3,22,23-Trihydroxystigmastan-6-one	462.37	C_{29} H_{50} O_4	485.356
1.536	Ornithine	132.09	C_5 H_{12} N_2 O_2	155.0805
1.62	Aprobarbital	210.10	C_{10} H_{14} N_2 O_3	211.1066
1.876	Cyclo(deltaAla-L-Val)	168.09	C_8 H_{12} N_2 O_2	169.0962
1.925	Biotin	244.09	C_{10} H_{16} N_2 O_3 S	245.0943
2.641	Gentisic acid	154.03	C_7 H_6 O_4	153.0191
2.674	Resorcinol	110.04	C_6 H_6 O_2	109.0292
3.257	Pirimicarb	238.14	C_{11} H_{18} N_4 O_2	261.1297
3.422	Butoctamide hydrogen succinate	315.20	C_{16} H_{29} N O_5	316.2108
4.017	Maculosin	260.12	C_{14} H_{16} N_2 O_3	261.1228
4.267	2-Dodecylbenzenesulfonic acid	326.19	C_{18} H_{30} O_3 S	349.1816
4.305	Rhodoxanthin	562.38	C_{40} H_{50} O_2	585.3725

4.527	Benzoic acid	122.04	$C_7 H_6 O_2$	121.0292
4.779	L,L-Cyclo(leucylprolyl)	210.14	$C_{11} H_{18} N_2 O_2$	211.1433
4.849	L-alpha-Amino-1H-pyrrole-1hexanoic acid	196.12	$C_{10} H_{16} N_2 O_2$	241.1193
4.958	o-Cresol	108.06	$C_7 H_8 O$	107.0498
4.972	Epirubicin	543.16	$C_{27} H_{29} N O_{11}$	566.1613
5.02	Erinacine P	492.27	$C_{27} H_{40} O_8$	493.2793
5.512	Cyclo(L-Phe-L-Pro)	244.12	$C_{14} H_{16} N_2 O_2$	245.1274
5.762	Geranylgeranylcysteine	407.25	$C_{23} H_{37} N O_3 S$	430.2432
6.136	(2S,4R)-4-(9H-Pyrido[3,4b]indol-1-yl)-1,2,4-butanetriol	272.12	$C_{15} H_{16} N_2 O_3$	271.1092
6.627	Glucocaffeic acid	342.09	$C_{15} H_{18} O_9$	365.0806
7.318	8,10-Nonacosanedione	436.43	$C_{29} H_{56} O_2$	241.2033
7.867	Acetyl tributyl citrate	402.22	$C_{20} H_{34} O_8$	403.2289
7.945	(1R,2R,4S)-p-Menthane-1,2,8triol 8-glucoside	350.19	$C_{16} H_{30} O_8$	373.1825
8.083	Spironolactone	416.20	$C_{24} H_{32} O_4 S$	417.2085
8.215	Ethyl (3R,5Z)-3-hydroxy-5octenoate	186.13	$C_{10} H_{18} O_3$	185.1182
8.221	16alpha,17-Dihydroxypregn-4ene-3,20-dione cyclic acetal with 2-furyl methyl ketone	438.25	$C_{27} H_{34} O_5$	461.2343
8.268	Ophiobolin F	358.32	$C_{25} H_{42} O$	437.2407
8.338	β-methasone dipropionate	504.25	$C_{28} H_{37} F O_7$	505.2606
8.354	9,13-Dihydroxy-4megastigmen-3-one 9glucoside	388.21	$C_{19} H_{32} O_8$	387.2052
8.403	Ipecac (Emetine)	480.30	$C_{29} H_{40} N_2 O_4$	525.2934
8.409	1-(4-Methoxyphenyl)-3-(4morpholinyl)-1-propanone	249.14	$C_{14} H_{19} N O_3$	248.1295
8.823	(+)-Ligballinol	298.12	$C_{18} H_{18} O_4$	297.1142
9.443	Oleandolide	386.23	$C_{20} H_{34} O_7$	387.234
9.555	4-Fluoro-17betahydroxyandrost-4-en-3-one propionate	362.23	$C_{22} H_{31} F O_3$	385.2183
10.825	Embelin	294.18	$C_{17} H_{26} O_4$	293.177
10.83	N'-Nitrosoanabasine	191.11	$C_{10} H_{13} N_3 O$	236.1063
10.862	Procarbazine	221.16	$C_{12} H_{19} N_3 O$	220.1472
11.664	Nigakilactone B	392.22	$C_{22} H_{32} O_6$	415.2097
11.969	Cyclopiazonic acid	336.15	$C_{20} H_{20} N_2 O_3$	337.1537
12.009	202-791	358.13	$C_{17} H_{18} N_4 O_5$	393.1004
12.294	beta-Cyclopiazonate	338.16	$C_{20} H_{22} N_2 O_3$	337.1568
13.69	Poriferastane skeleton	400.41	$C_{29} H_{52}$	479.3241

13.849	3-keto stearic acid	298.25	$C_{18}H_{34}O_3$	297.2439
13.901	Decylubiquinol	324.23	$C_{19}H_{32}O_4$	323.2238
15.956	Lauryl hydrogen sulfate	266.16	$C_{12}H_{26}O_4S$	265.1487
16.037	Lucidenic acid M	462.30	$C_{27}H_{42}O_6$	485.2883
16.815	Pubesenolide	458.30	$C_{28}H_{42}O_5$	481.2908
17.113	Red chlorophyll catabolite	626.27	$C_{35}H_{38}N_4O_7$	671.2703
17.116	Linalyl caprylate	280.24	$C_{18}H_{32}O_2$	279.2339
17.125	Neomycin B	614.31	$C_{23}H_{46}N_6O_{13}$	637.304
17.782	Bolegrevilol	440.29	$C_{28}H_{40}O_4$	463.2807
17.837	3,5-Cyclo-5alpha,17alphapregn-20-yne-6beta,17-diol	314.22	$C_{21}H_{30}O_2$	315.2309
17.981	Cyanidin 3-(diferuloylsophoroside) 5glucoside	274.21	$C_{17}H_{26}N_2O$	309.1756
18.089	beta-tocotrienol	410.32	$C_{28}H_{42}O_2$	411.3248
18.172	Petroselinic acid	282.26	$C_{18}H_{34}O_2$	281.2498
18.193	PG(16:1(9Z)/18:3(9Z,12Z,15Z))	742.48	$C_{40}H_{71}O_{10}P$	741.4752
18.405	3-Hydroxy-1-phenyl-1eicosanone	388.34	$C_{26}H_{44}O_2$	411.3243
18.737	Tetradecyl sulfate	294.19	$C_{14}H_{30}O_4S$	353.2019
18.979	3-(2,4-Cyclopentadien-1ylidene)pregn-4-en-20-one	362.26	$C_{26}H_{34}O$	397.2283
19.141	Silafluofen	408.19	$C_{25}H_{29}FO_2Si$	431.1771
19.304	Sarcostin	382.24	$C_{21}H_{34}O_6$	441.2549
19.559	Glutathionylspermidine	434.23	$C_{17}H_{34}N_6O_5S$	479.2268
20.701	2-(methylthio)ethyl glucosinolate	393.03	$C_{10}H_{19}NO_9S_3$	471.9454

4.3.7 Molecular Docking

To develop effective inhibitors and drugs against cancer, specific types of RTKs, including VEGFR, PDGFR, FGFR, ALK, AXL, EGFR, and IR, having mutations at specific locations, have been selected. In order to elucidate the inhibitory efficacy of compounds derived from *Streptomyces clavuligerus* against different RTKs, molecular docking and molecular dynamics simulation techniques were conducted. As a point of reference, pazopanib was utilized as the standard drug for comparative purposes for all the RTKs studied (Pottier et al., 2020).

Based on the docking results, ligands with superior binding scores and stronger binding interactions with RTKs receptors compared to the standard drug were identified. Previously, these ligands have also been demonstrated to have anticancer activity. Subsequently, further evaluation was carried out on PDGFR, VEGFR, and FGFR receptors using the ligands meeting the mentioned criteria. However, the ligands did not exhibit better binding affinity than the standard drug for other receptors such as ALK, AXL, EGFR, and IR. For the VEGFR receptor, the selected ligands were Dodecaprenyl phosphate-galacturonic acid (DPGA), Naringenin (Nar), and Epirubicin (Epi). For the FGFR receptor, Neomycin B (NeoB), Dodecaprenyl phosphate-galacturonic acid, and Epirubicin were chosen, and for the PDGFR receptor, Epirubicin, Neomycin B and Monotropein (Mono) were selected as the preferred ligands (Ahamad et al., 2014; Attanzio et al., 2018; Cabral-Romero et al., 2021; Chong et al., 2020; Hosseini Abari et al., 2021; Hu, 2001; F. Wang et al., 2014; R. Wang et al., 2019).

The molecular docking analysis of ligands with VEGFR-2 receptor demonstrated that the top three ligands, DPGA (-10.895), Naringenin (-10.151), and Epirubicin (-9.766), exhibited superior binding scores when compared to the standard ligand Pazopanib (-7.155), as indicated in Table 4.3.

Table 4.3: Binding energy and interaction analysis of the top 3 secondary metabolites *Streptomyces clavuligerus* and standard ligand Pazopanib with various Receptor Tyrosine Kinases (RTKs).

Target	Compound name	Docking score	H-bond	Hydrophobic interaction
FGFR	Neomycin B	-10.440	Asp630, Asn617, Arg616, Ala553, Leu473, Glu475	Ala629, Leu619, Lys503, Ala501, Arg483, Val481, Phe478, Ala477, Gly476, Gly474, Glu560, Asn557, Gly556, Lys555, Ala554, Cys552
	Dodecaprenyl phosphate-galacturonic acid	-10.378	Asp630, Arg616, Asn617, Glu475, Asn557	Leu473, Gly474, Gly476, Phe478, Val481, Arg483, Ala629, Leu619, Lys503, Ala501, Glu560, Gly556, Ala554, Ala553, Cys552, Glu551, Met550, Ile534

	Epirubicin	-10.024	Ala553, Ala554, Glu475	Leu619, Ala501, Lys503, Ile534, Arg483, Val481, Ala629, Phe478, Gly474, Leu473, Glu560, Asn557, Gly556, Lys555, Cys552, Glu551, Met550
	Standard-Pazopanib	-7.069	Arg483, Ala553, Ala554	Arg616, Asn617, Leu619, Ile534, Ala629, Asn557, Gly556, Lys555, Cys552, Glu551, Val481, Phe478, Glu475, Leu473, Ala501, Lys503
PDGFR	Epirubicin	-10.325	Leu599, Tyr679, Cys677	Gly600, Arg597, Leu825, Cys835, Val607, Val658, Ile674, Ala625, Glu675, Tyr676, Phe678, Gly680, Asp681, Asn684
	Neomycin B	-9.632	Arg597, Asp681, Cys677, Glu675, Arg822, Asn823	Ala625, Val607, Cys835, Asp836, Leu825, Gly600, Leu599, Val598, Asn684, Gly680, Tyr679, Tyr676, Val658, Ile674
	Monotropein	-8.731	Cys677, Glu675, Asn823, Asp836	Asp681, Gly680, Tyr676, Ile674, Ala625, Val658, Leu599, Gly600, Val607, Cys835, Leu825, Arg822
	Standard-Pazopanib	-3.379	Asn823, Asp836, Cys677	Asp681, Gly680, Tyr679, Phe678, Tyr676, Glu675, Ile674, Val658, Cys835, Leu825, Arg822, Ala625, Lys627, Glu644, Leu599, Gly600, Ser601, Val607
VEGFR	Dodecaprenyl phosphate-galacturonic acid	-10.895	Asp1046, His1026, Arg1027	Cys1045, Ile1044, Asp1028, Ile1025, Cys1024, Phe1047, Gly1048, Ala1050, Ile1053, Ile888, Leu889, Ile892, Leu1019, Val848, Lys868, Ala866, Gly922, Cys919, Phe918, Glu917, Thr916, Leu1035, L840, Tyr1059, Pro1068, Val898, Val899
	Naringenin	-10.151	Cys919	Cys1045, Asp1046, Phe1047, Val914, Thr916, Glu917, Phe918, Lys920, Gly922, Gly841, Leu840, Val848, Ala866, Lys868, Leu889, Val899, Leu1035
	Epirubicin	-9.766	Lys868, Glu885, Ser884, Ala881, Ile1025, His1026, Arg1027	Val899, Val898, Thr916, Val914, Ile892, Leu889, Ile888, Leu882, Leu1019, Cys1024, Ile1044, Cys1045, Asp1046, Gly1048, Leu1049
	Standard-Pazopanib	-7.155	Phe(pi-pi)	Leu1035, Ala866, Lys868, Glu885, Ile888, Leu889, Leu1019, Ile892, Ile1044, Cys1045, Asp1046, Val898, Val899, Thr916, Glu917, Phe918, Cys919, Gly922, Val848, Gly841, Leu840

The study revealed that Pazopanib showed no hydrogen bond interactions with the VEGFR receptor. However, it participated in a pi-pi interaction through its pyrimidine ring with the Phe1047 residue of the hinge region of the VEGFR receptor (Elkaeed et al., 2022). The ligand DPGA was found to retain a hydrogen phosphate group linked to the galacturonic acid moiety. Through this phosphate group, the ligand formed hydrogen bond interactions with the amino acid residues Arg1027 and His1026 of VEGFR. Additionally, the galacturonic acid moiety of the ligand also participated in hydrogen bonding, forming an interaction with the amino acid residue Asp1046 residue of the DFG motif (triad Asp-Phe-Gly) in the activation loop (M. A. McTigue et al., 1999; Sanphanya et al., 2013). Naringenin was observed to interact with the Cys919 residue in the hinge area of VEGFR via its keto and hydroxyl groups located on the benzopyran ring (Modi & Kulkarni, 2019). Epirubicin was observed to participate in hydrogen bond interactions with the amino acid residue Lys868 through its anthraquinone ring and NH2 group of the daunosamine ring (ring D), forming two hydrogen bonds with the residues Ser884 and Ala881. The anchor region of Epirubicin, which is attached to the ring A of anthraquinone, also formed three hydrogen bonds with the amino acid residues Arg1027, His1026, and Ile1025 in the activation loop (M. A. McTigue et al., 1999).

The molecular docking study of FGFR with the ligand derived from *Streptomyces clavuligerus* revealed that the ligands, namely Neomycin B (-10.440), DPGA (-10.378), and Epirubicin (-10.024), exhibited significantly better binding scores than the standard drug Pazopanib (-7.069). It was found that the standard ligand Pazopanib interacted with the amino acid residues Ala554 and Arg483 via its sulfonamide group and with Ala553 in the hinge region of FGFR through its pyrimidine ring (Tucker et al., 2014). Additionally, it formed another hydrogen bond with Ala553 through the amino group linked with the sulfonamide group and the pyrimidine ring. Neomycin B is a complex aminoglycoside

compound composed of four moieties, including D-neosamine, 2-deoxystreptamine, D-ribose sugar, and L-neosamine, and contains the largest number of free amino groups (six). The molecular docking analysis revealed that it formed hydrogen bond interactions with several amino acid residues of FGFR, including Gly474 and Leu473 via D-neosamine, Ala553 via 2-deoxystreptamine, Arg616, and Glu475 via D-ribose, and Asp630 (DFG motif), Asn617, and Glu475 via L-neosamine (Modh et al., 2022, 2023). These results suggest that Neomycin B has the potential to serve as a promising lead compound for the development of FGFR-targeting therapeutics. The ligand DPGA exhibited two hydrogen bond interactions with Asn557 and Arg616 through its hydrogen phosphate group. Its galacturonic acid moiety also formed several hydrogen bond interactions with amino acid residues Glu475, Asp630, Arg616, and Asn617 in the active site of the FGFR receptor (Dehghanian & Alavi, 2021).

The ligand Epirubicin exhibited a hydrogen bond interaction with the Ala553 amino acid residue through its hydroxyl and keto group present in the anthraquinone ring. The hydroxyl group of the daunosamine ring (ring D) also formed hydrogen bonds with residue Glu475. In addition, the hydroxyl group present in the anchor region of Epirubicin made hydrogen bonds with the Ala554 residue (Badichi Akher et al., 2019; Saini et al., 2024). Docking studies revealed that among the ligands screened for PDGFR receptor, Epirubicin (-10.325), Neomycin B (-9.632), and Monotropein (-8.731) exhibited superior binding scores compared to the standard drug pazopanib (-3.379). Upon investigation, it was observed that the standard ligand pazopanib interacted with Asn823 via its sulfonamide group and with Cys677 via its indazole ring. Additionally, a hydrogen bond was formed with Asp836 via the amino group attached between the sulfonamide and pyrimidine ring. Epirubicin was found to interact with the Cys677 amino acid residue of

the DGF activation loop region of the PDGFR receptor through its hydroxyl and keto groups present in the anthraquinone ring (Nemaysh & Luthra, 2017).

The hydroxyl group of the daunosamine ring (ring D) also formed hydrogen bonds with residue Leu599. Moreover, the hydroxyl group present in the anchor region of the ligand made hydrogen bonds with the Tyr679 residue of the receptor.

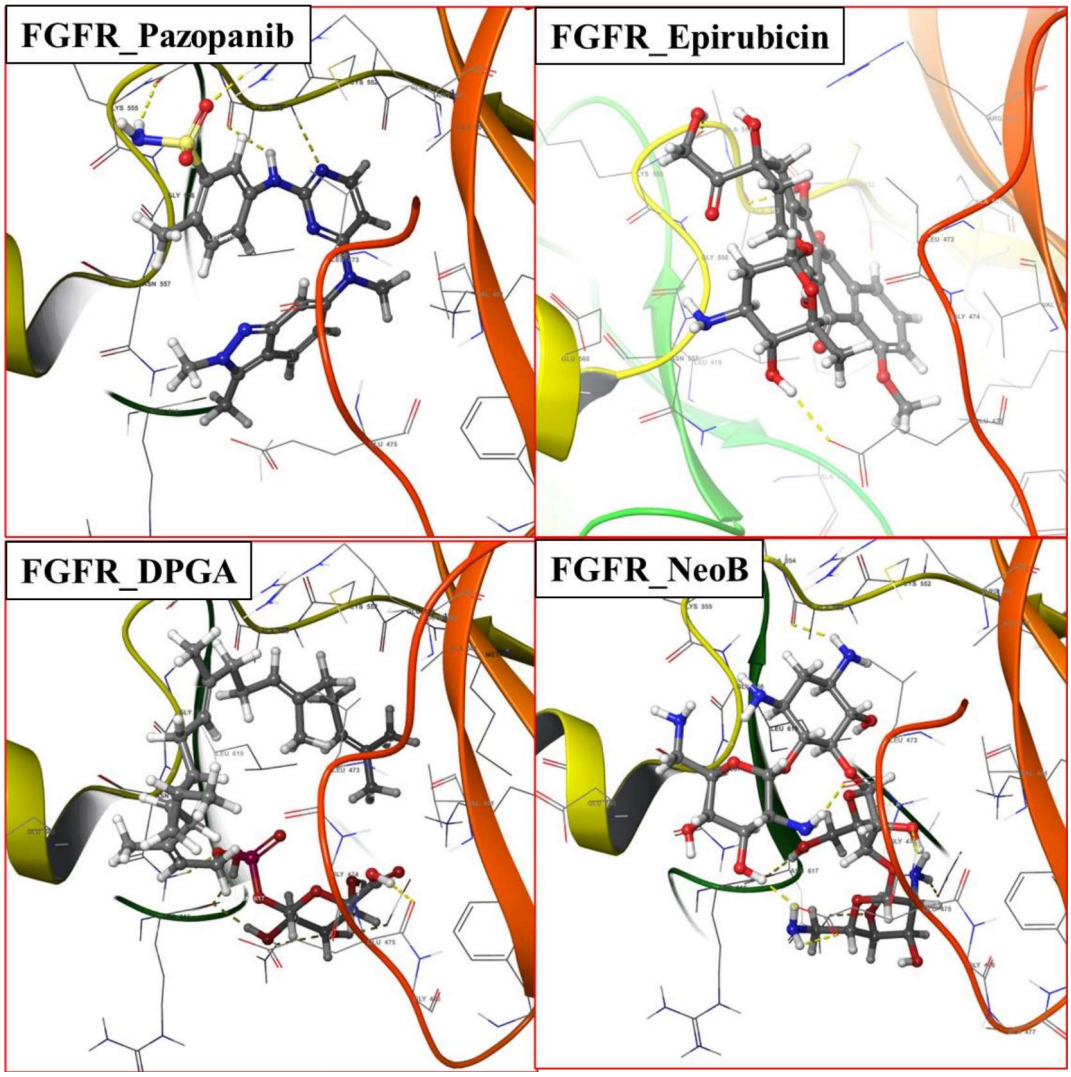

Figure 4.7.1: 3D molecular docking interactions of top ligands and standard drug Pazopanib with FGFR Receptor Tyrosine Kinases

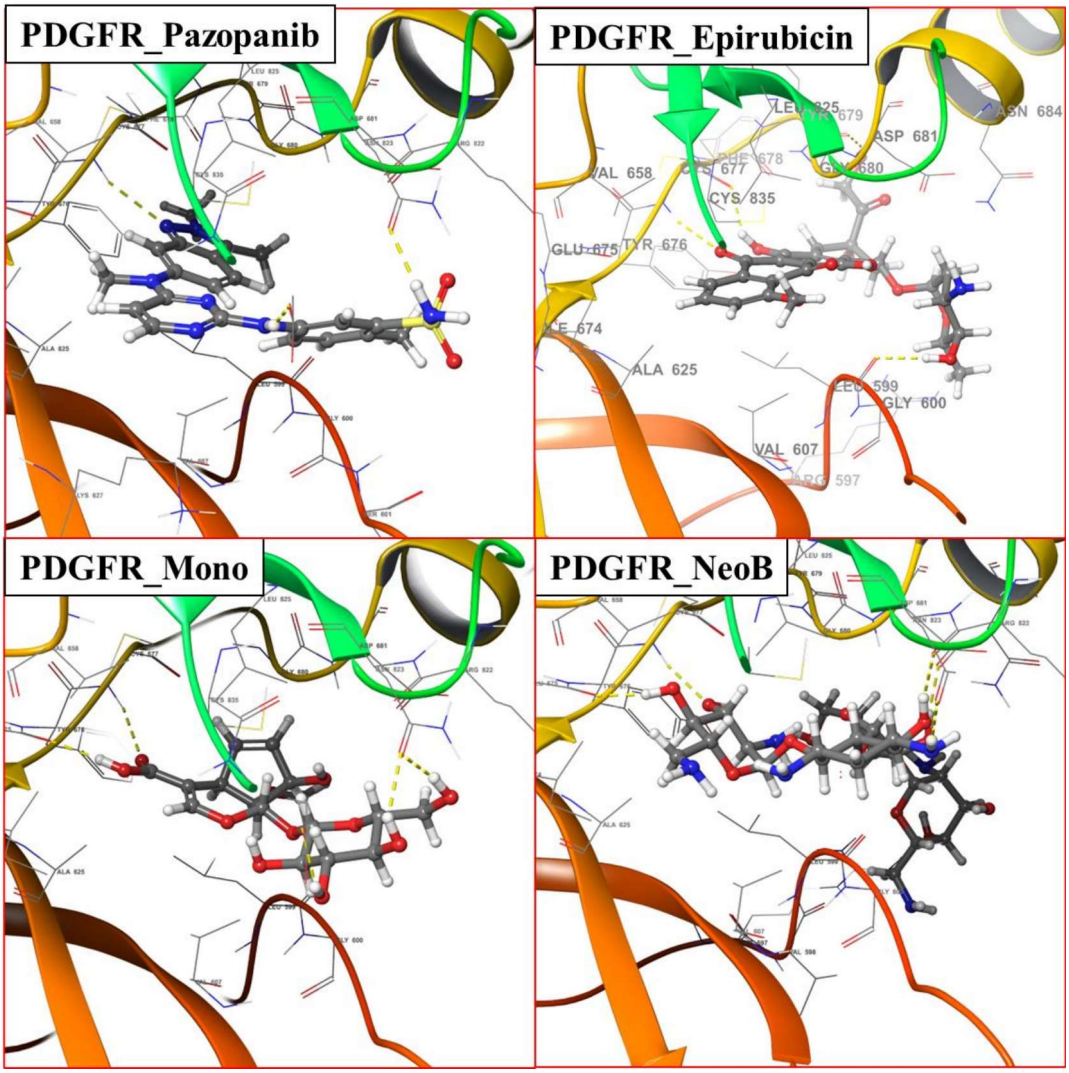

Figure 4.7.2: 3D molecular docking interactions of top ligands and standard drug Pazopanib with PDGFR Receptor Tyrosine Kinases

The compound Neomycin B exhibited hydrogen bond interactions with several amino acid residues of the PDGFR receptor. Specifically, its D-neosamine moiety formed hydrogen bonds with Glu675 and Cys677 (DGF activation loop region of the PDGFR receptor), while its 2-deoxystreptamine moiety interacted with Asn823 and Arg822. The D-ribose moiety of Neomycin B made a hydrogen bond with Asp681, and the L-neosamine group formed a hydrogen bond with Arg597 (Nemaysh & Luthra, 2017). Monotropein exhibited hydrogen bond interactions with Glu675 and Cys677 residues of the PDGFR receptor through its carboxylic group on the pyran ring.

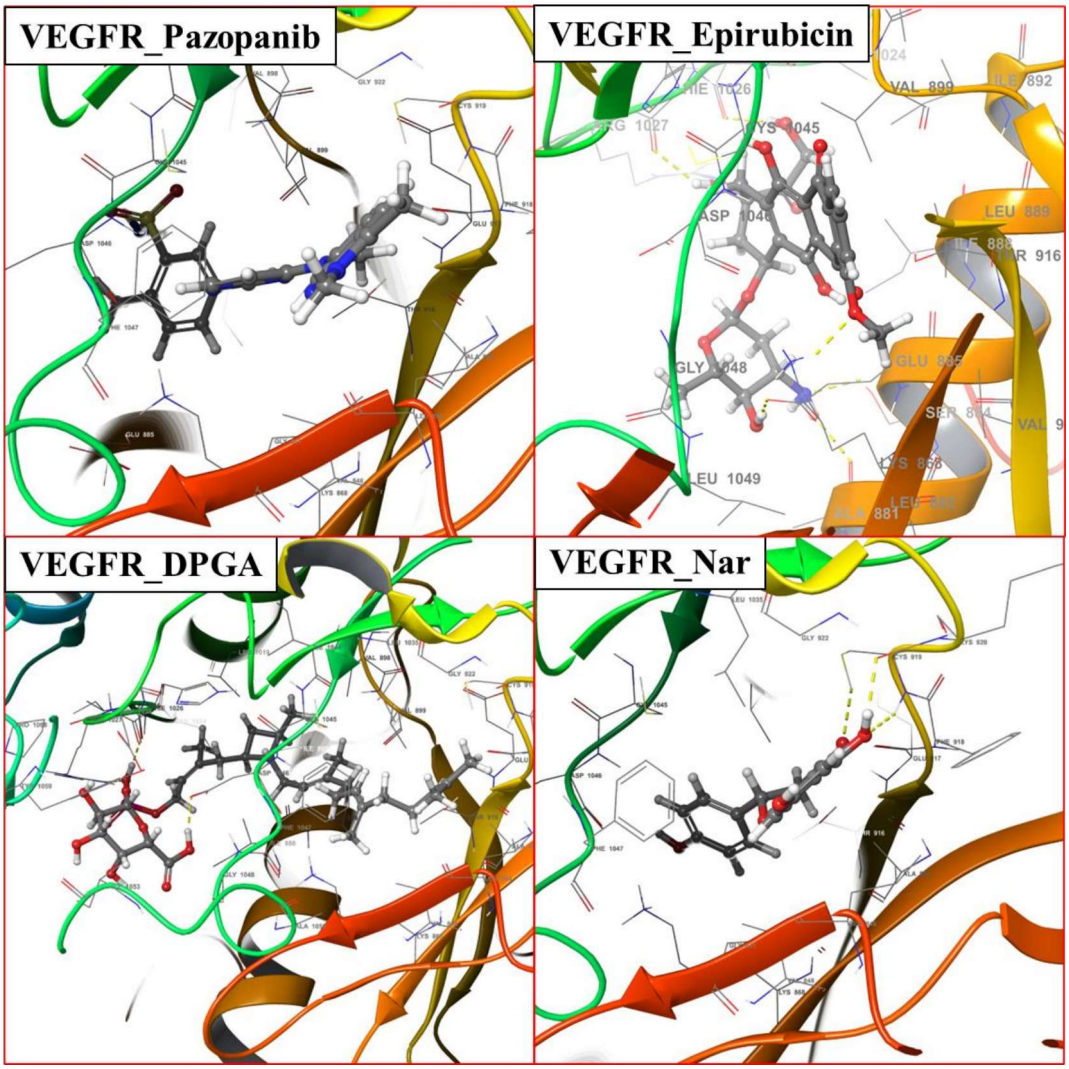

Figure 4.7.3: 3D molecular docking interactions of top ligands and standard drug Pazopanib with VEGFR Receptor Tyrosine Kinases

Additionally, the hydroxyl and hydroxymethyl groups on the oxane ring of Monotropein formed hydrogen bond interactions with the Asn823 and Asp836 residues of the receptor. The receptor-ligand docking interactions in 3D are represented in Figures 4.7.1 to 4.7.3.

4.3.8 Molecular dynamics simulation

Based on molecular dynamic simulation results, Figure 4.8 illustrates the RMSD of all RTK proteins in the Apo state, complex with ligands and standard drug pazopanib. The root mean square deviation (RMSD) of the C-alpha atoms was computed to evaluate the dynamic behaviour of the complex throughout the simulation trajectories. The findings

demonstrated that all the protein-ligand complexes maintained a consistent RMSD throughout the simulation, implying high stability.

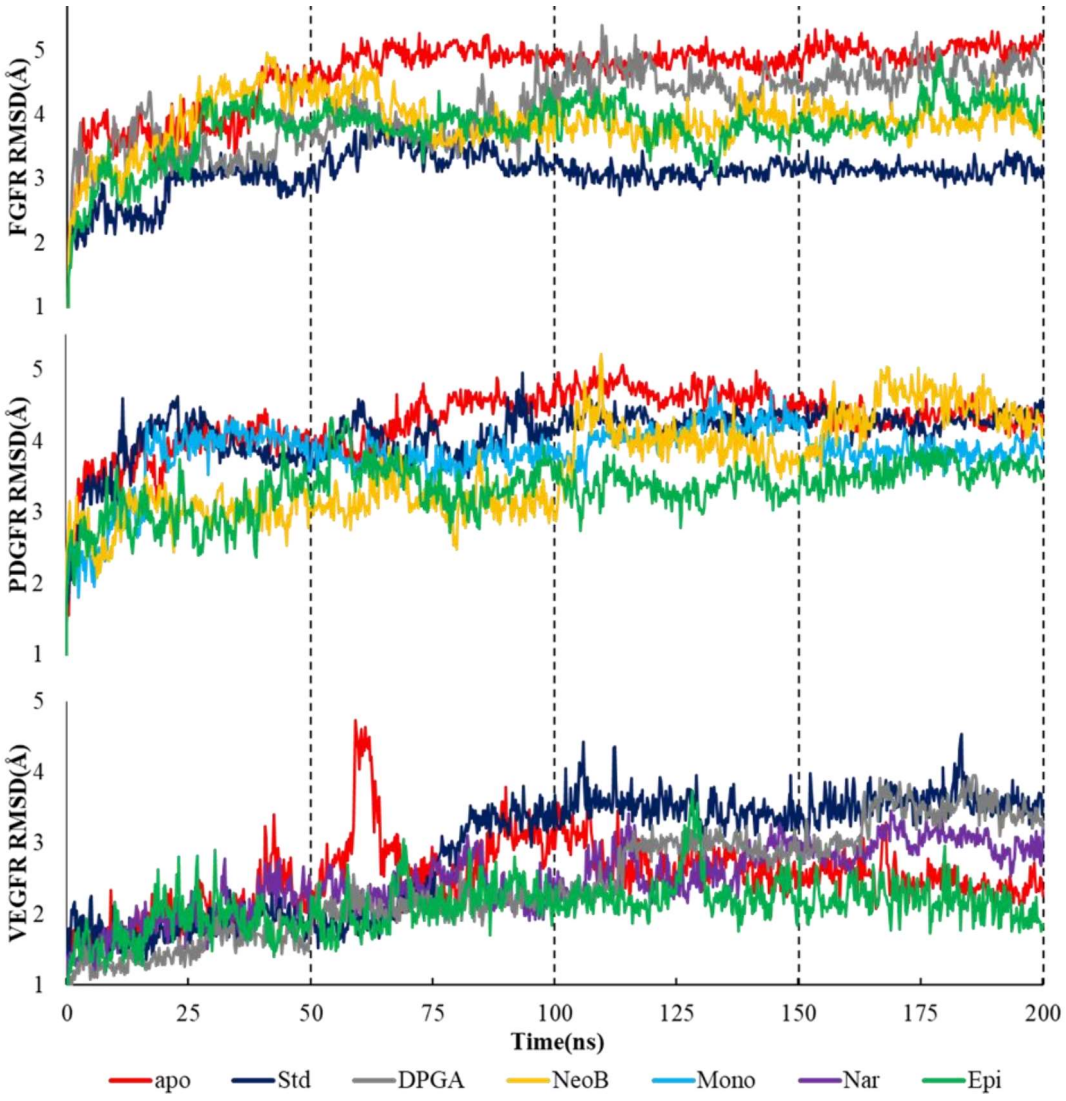

Figure 4.8: Root Mean Square Deviation (RMSD) profiles of the respective three targets RTKs in Apo state, in complex with ligand and Std (protein with Pazopanib) during Molecular Dynamics.

The protein-ligand complex comprising ligand Epirubicin bound to the VEGFR receptor demonstrated the highest stability and exhibited the lowest deviation compared to ligand Naringenin, DPGA, and the standard drug pazopanib. For the PDGFR protein, ligands Epirubicin and Neomycin B initially fluctuated but maintained stability throughout the simulation. Furthermore, the average RMSD of all the ligands was lower than that of

pazopanib (4.09 A˚). In the case of FGFR, all ligands displayed higher deviation than the standard drug (3.09 A˚), and ligand epi exhibited lower deviation than DPGA and Neomycin B. The RMSD trend of all the complexes reached a plateau after 75 ns, indicating that the complexes remained stable and rigid throughout the simulation period.

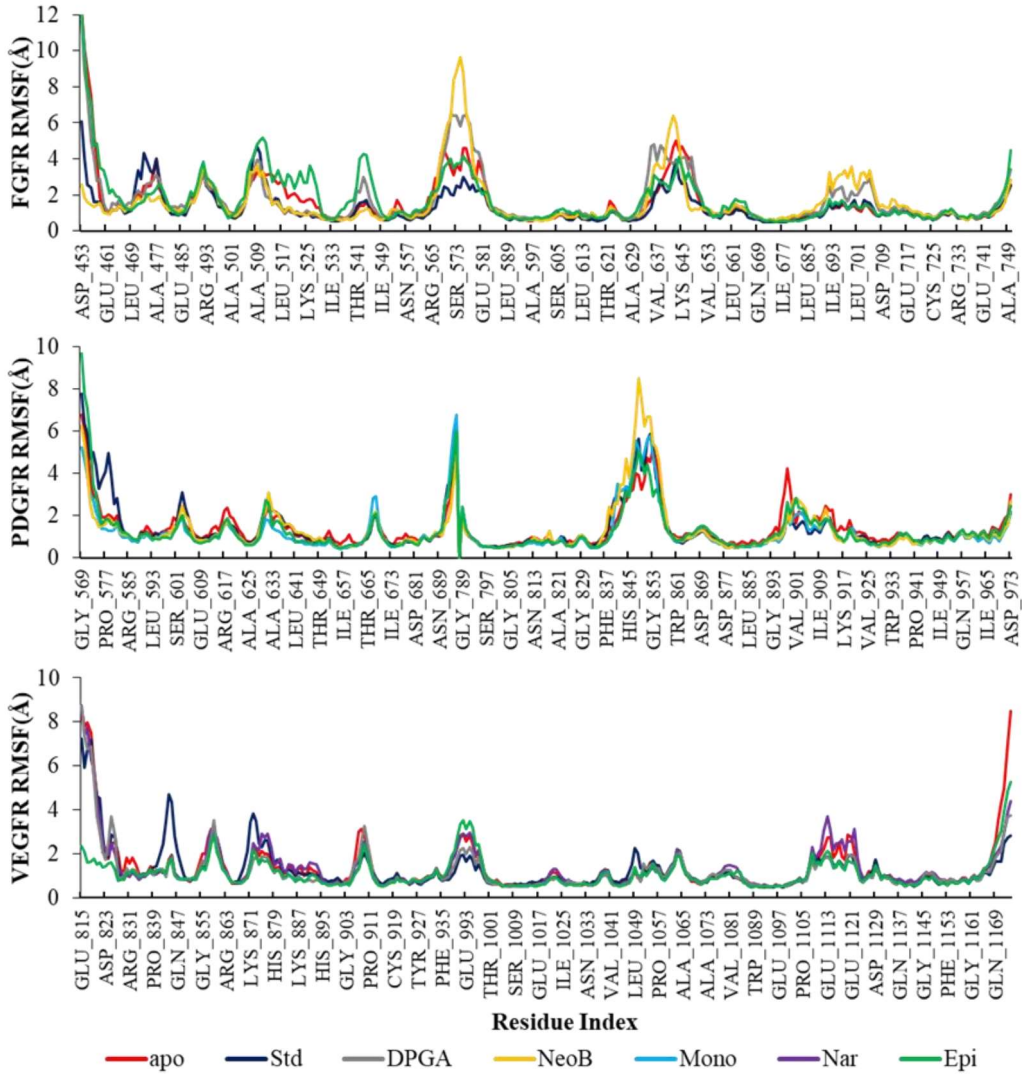

Figure 4.9: Root Mean Square Fluctuations (RMSF) profiles of the respective three targets RTKs in Apo state, in complex with ligand and Std (protein with Pazopanib) during Molecular Dynamics.

In dynamic conditions, amino acids in proteins constantly fluctuate, resulting in conformational changes in the protein structure. To assess this phenomenon, an RMSF plot was utilized. The RMSF plot revealed higher fluctuations at the protein's terminal

ends (C- and N-terminals) rather than the central region. Moreover, the alpha-helix structure exhibited greater rigidity compared to the terminal and loop regions. Remarkably, the amino acid residues located in the binding site of the protein-ligand complex displayed minimal fluctuations, as evidenced by Figure 4.9. This observation indicated that most amino acid residues had an RMSF value of less than 2.5 A˚, providing further evidence of the complex's stability. Furthermore, it demonstrated that protein secondary structures, such as alpha-helices and beta-sheets, remained highly rigid throughout the simulation.

The solvent-accessible surface area (SASA) of the docked complexes was analyzed to assess the degree of expansion or unfolding of the protein. An initial increase in the SASA value indicates expansion in the protein surface area, which could be due to unfolding. The Epirubicin ligand demonstrated high stability and remained mostly within the binding cavity of the FGFR protein, as indicated by its SASA profile being similar to that of the standard drug. On the other hand, the SASA profiles of Neomycin B and DPGA showed initial expansion in the surface area of the FGFR from the beginning to 50 ns, followed by stabilization until 75 ns, and reaching a steady state thereafter. This trend was maintained until the completion of the simulation time, as depicted in Figure 4.10. For PDGFR protein, the standard drug exhibited fluctuations up to 75 ns before becoming stable. At the same time, Neomycin B and Epirubicin demonstrated higher SASA values, indicating that a greater portion of the drug remained outside of the binding pocket of the protein, where it was accessible to solvents. Moreover, it was observed that Monotropein demonstrated stability initially, but after 65 ns, it became highly unstable at the end of the simulation, indicating that most of the ligand came out of the binding pocket of the receptor. For the VEGFR receptor, Naringenin exhibited the lowest SASA value,

indicating that only a small portion of the ligand was accessible to water, while DPGA and Epirubicin demonstrated comparable SASA values to standard ligands.

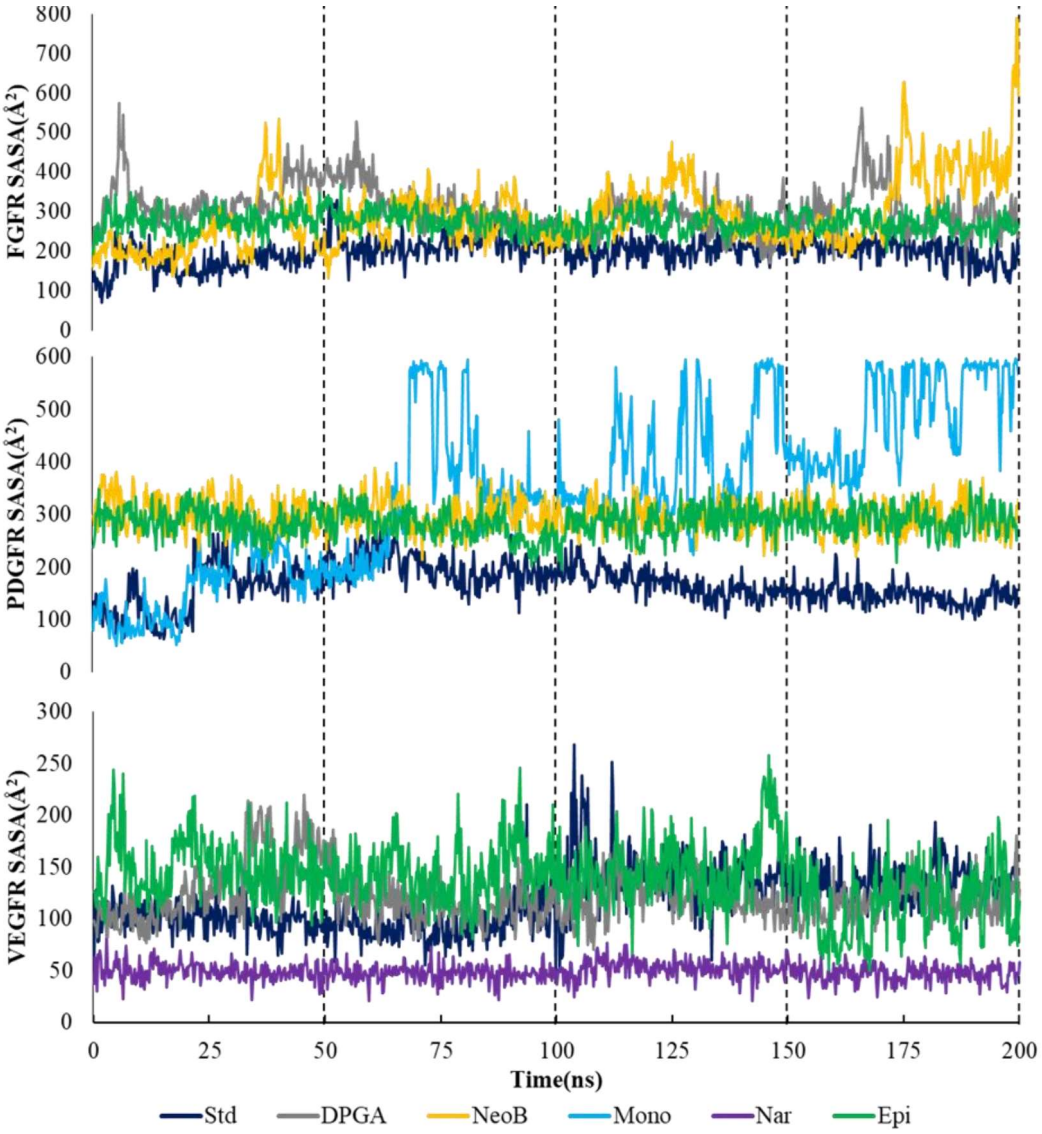

Figure 4.10: Solvent Accessible Surface Area (SASA) profiles of the respective three targets RTKs in complex with ligand and Std (protein with Pazopanib) during Molecular Dynamics.

The radius of gyration (Rg) of ligands is a parameter that reflects their extent of expansion or compactness during simulation. A low Rg profile implies its compact nature, whereas a higher Rg profile suggests greater extendedness of ligands.

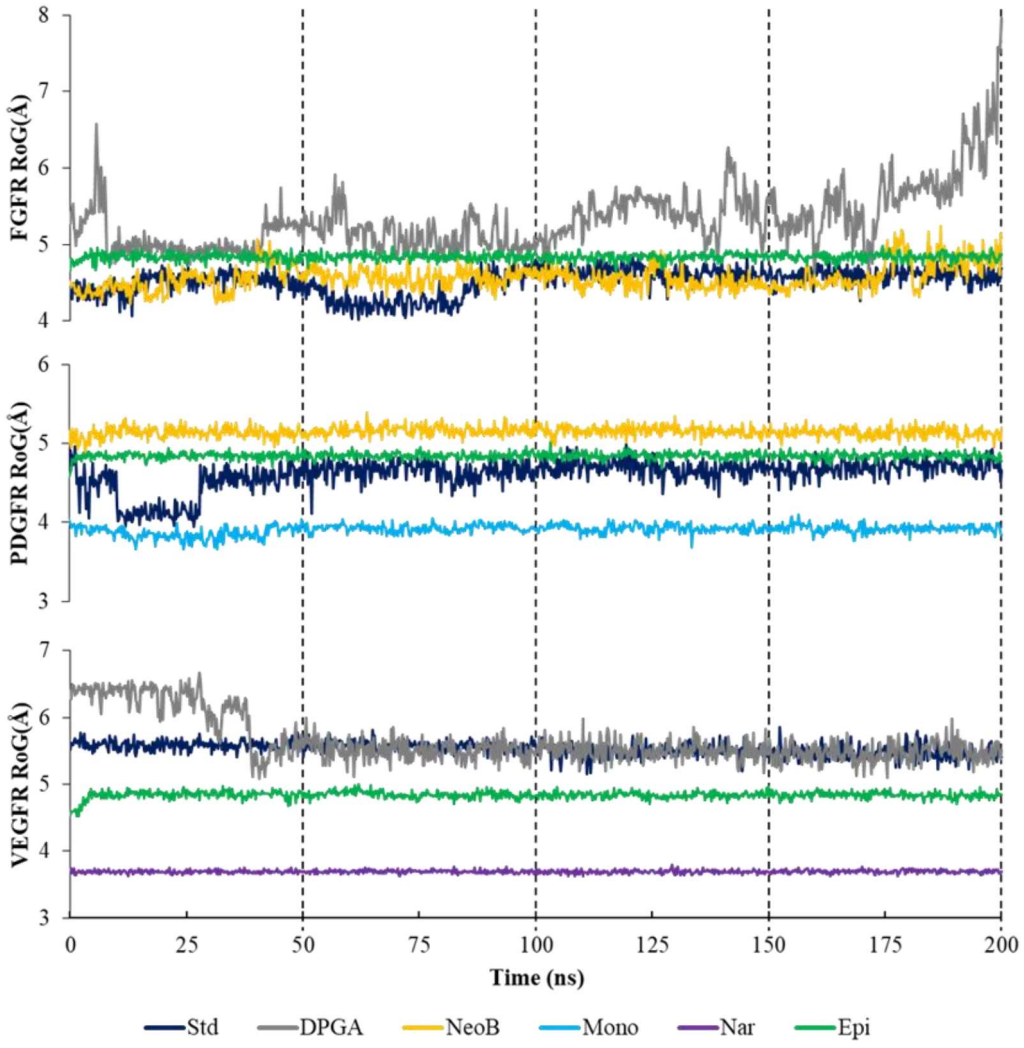

Figure 4.11: Radius of Gyration (Rg) profiles of the respective three targets RTKs in complex with ligand and Std (protein with Pazopanib) during Molecular Dynamics.

In the FGFR interaction, Epirubicin and DPGA exhibited highly stable and similar Rg values to the standard, indicating that the ligands remained compact and rigid during the simulation due to their aromatic structure.In contrast, Neomycin B displayed a high and fluctuating Rg compared to the standard. For PDGFR, Epirubicin and Neomycin B showed higher Rg values than the standard, while Monotropein had a lower Rg value. Regarding VEGFR, DPGA was initially unstable for the first 40 ns but then became stable and followed a similar trend with Rg value as the standard, while ligands Naringenin and epi displayed stable Rg values and had lower values than the standard. Figure 4.11

demonstrates the Rg profile of the complex, which remained almost constant during the simulation, which was indicative of the ligand stability and rigid conformation throughout the simulation period.

During a 200 ns simulation, the formation of hydrogen bonds is seen, as shown in Figure 4.12**,** between ligands and amino acid residues of receptor tyrosine kinases (RTKs). These findings indicate that the standard drug pazopanib formed 1-5 hydrogen bonds with all three RTKs. DPGA and Epirubicin formed 1-7 and 1-6 hydrogen bonds with the FGFR receptor, respectively. Initially, Neomycin B formed 4-12 hydrogen bonds within the first 25 ns; however, the number of hydrogen bonds decreased and stabilized at 1-8 bonds for the remainder of the simulation. With the PDGFR receptor, Monotropein formed 1-7 hydrogen bonds until 60 ns, after which the number of hydrogen bonds decreased to 4. On the other hand, Neomycin B and Epirubicin interacted with the PDGFR receptor by forming 2-9 and 1-5 hydrogen bonds, respectively. Epirubicin and Naringenin formed 1-5 and 1-7 hydrogen bonds, respectively, with VEGFR. Interestingly, DPGA initially formed 4-9 hydrogen bonds within the first 25 ns but stabilized at 5 hydrogen bonds for the remainder of the simulation.

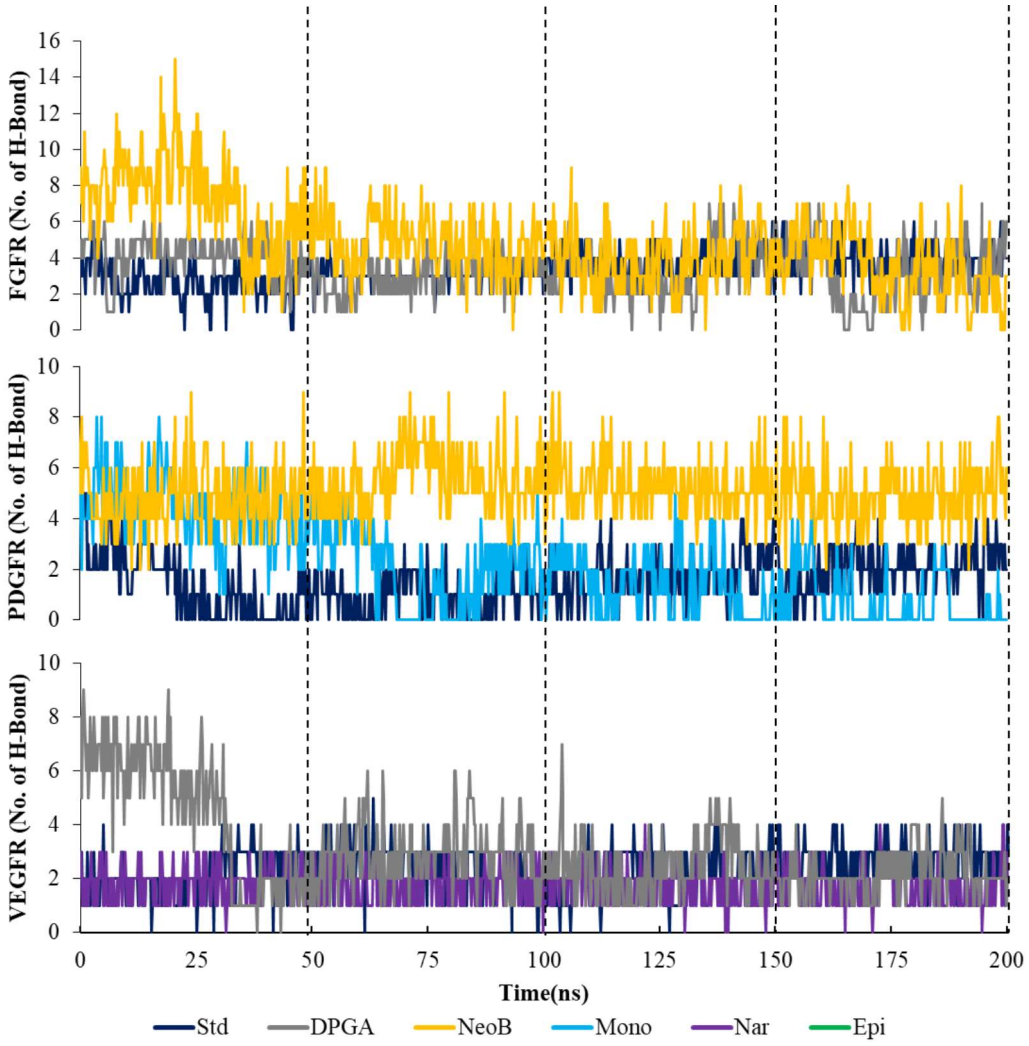

Figure 4.12: Number of Hydrogen Bond formation profiles of three targets RTKs in complex with ligand and Std (protein with Pazopanib) during Molecular Dynamics.

4.3.9 Protein-Ligand Interaction

The protein-ligand contacts have been investigated during a 200 ns MD simulation to examine the interactions between amino acid residues and ligands. These interactions include hydrogen bonding, hydrophobic, ionic, water bridging, and pi-pi stacking, which contribute to the compactness and stability of the inhibitor in the protein active site. A 2D plot is presented in Figures 4.13.1 to 4.13.3 that illustrates the interaction between ligands and the interacting residues of RTKs, along with their corresponding interaction percentages during the simulation.

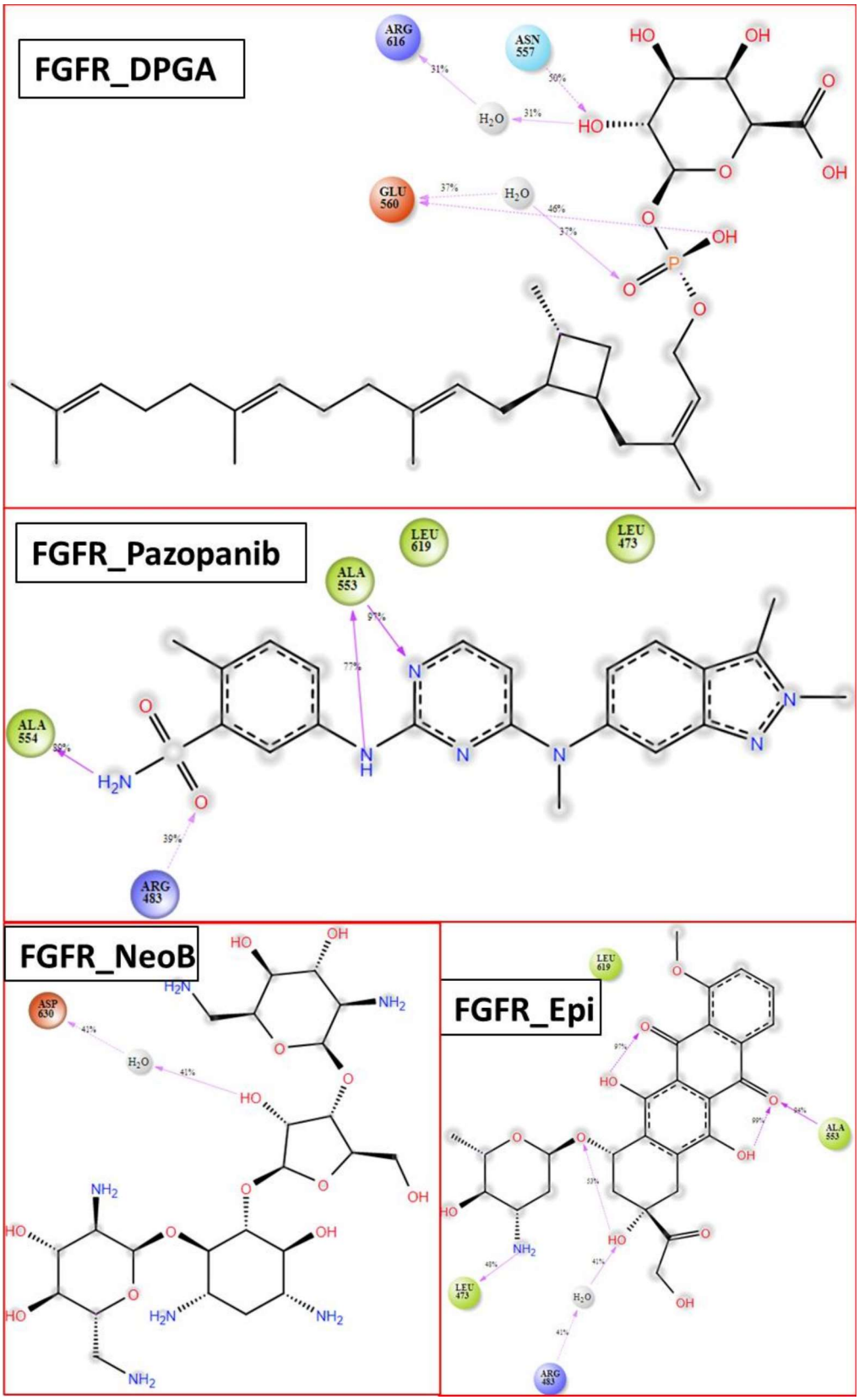

Figure 4.13.1: The 2D plot represents the protein-ligands interaction analysis of ligands and standard drug Pazopanib with interaction residue of FGFR and their interaction percentage during an MD simulation of 200 ns

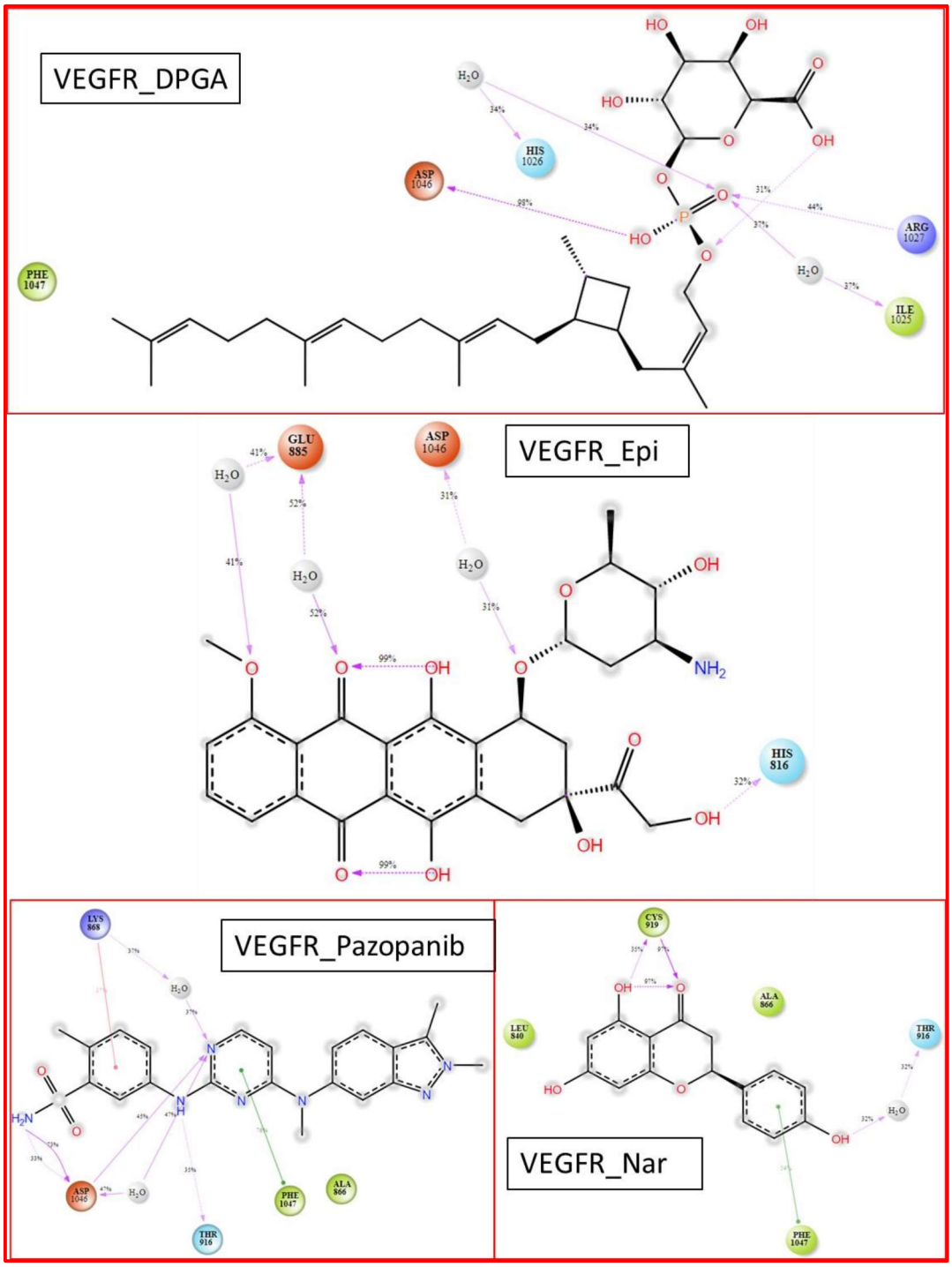

Figure 4.13.2: The 2D plot represents the protein-ligands interaction analysis of ligands and standard drug Pazopanib with interaction residue of VEGFR and their interaction percentage during an MD simulation of 200 ns

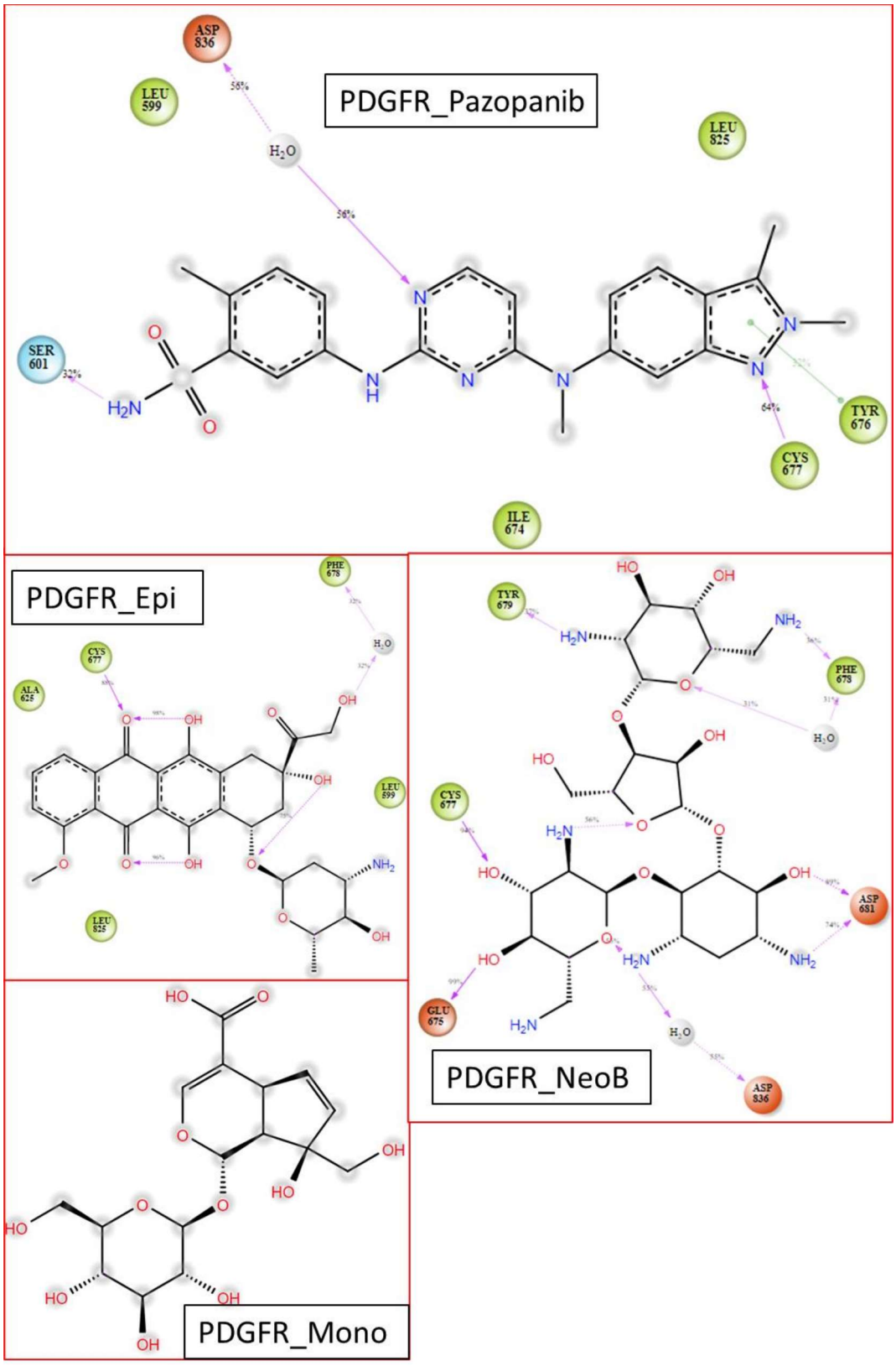

Figure 4.13.3. The 2D plot represents the protein-ligands interaction analysis of ligands and standard drug Pazopanib with interaction residue of PDGFR and their interaction percentage during an MD simulation of 200 ns

Standard ligand pazopanib did not exhibit any hydrogen bond interactions with the VEGFR receptor during molecular docking. However, MD simulation revealed that the pyrimidine ring of the pazopanib established 45% hydrogen bond interactions and 47% water bridge interactions with the Asp1046 residue present in the activation loop of the VEGFR receptor (Sanphanya et al., 2013). Additionally, the pyrimidine ring maintained 76% pi-pi interactions with the amino acid residue Phe1047, and the benzene ring maintained 37% pi-pi interactions with the Lys868 residue. The phosphate moiety of the DPGA ligand formed hydrogen bond interactions with the Arg1027 residue (44%), Asp1046 residue (98%), and a 37% water-mediated interaction with the Ile1025 residue of the VEGFR receptor. The Naringenin ligand made two hydrogen bond interactions with the Cys919 residue in the ATP binding pocket of VEGFR via its keto and hydroxyl groups located on the benzopyran ring with 97% and 35% probability, respectively. Its phenolic group revealed water-bridge interaction with Thr916 and 54% pi-pi interaction with Phe1047. The Epirubicin ligand was observed to mediate two water-bridge interactions with the Glu885 (DGF motif) of VEGFR with 52% and 41% probability through its anthraquinone ring. Additionally, its daunosamine ring formed a 31% water-mediated interaction with Asp1046.

In a molecular simulation study of FGFR, the interactions of standard ligands Pazopanib, Neomycin B, DPGA, and Epirubicin with specific residues of the receptor were analyzed. The results showed that Pazopanib exhibited 89% hydrogen bond interactions with residue Ala554 through its sulfonamide group and 97% H-bond interactions through its pyrimidine ring. Neomycin B formed a 41% water-bridging interaction with residue Asp630 in the DGF motif of FGFR via its D-ribose sugar (Mahfuz et al., 2022). DPGA exhibited 46% hydrogen bond interactions with the Glu560 residue of the receptor through its phosphate moiety and 50% H-bond interaction with Asn557 via its

galacturonic acid moiety (Liang et al., 2012). Epirubicin demonstrated hydrogen bond interaction with the Ala553 amino acid residue through its hydroxyl and keto groups present in the anthraquinone ring. The hydroxyl group of the daunosamine ring also formed hydrogen bonds with residue Glu475. Additionally, the hydroxyl group present in the anchor region of Epirubicin made a hydrogen bond with the Ala554 residue of the FGFR receptor.

Based on a molecular dynamics simulation study of PDGFR, it was revealed that the pyrimidine ring of Pazopanib formed a 56% water-bridge interaction with the Asp836 protein residue. Epirubicin mediated 88% hydrogen bond interaction through its hydroxyl group present in the anthraquinone ring with Cys677, while Monotropein did not form any hydrogen bond interaction with the PDGFR protein. Neomycin B demonstrated 99% hydrogen bond interaction with Glu675 and 94% interaction with the Cys677 residue of the PDGFR receptor through its D-neosamine group. Additionally, its 2-deoxystreptamine moiety mediated 89% and 74% interaction with the Asp681 residue at the hinge region of the PDGFR receptor (Nemaysh & Luthra, 2017). These findings provide valuable insights into the molecular interactions of these drugs with PDGFR, VEGFR, and FGFR proteins and can contribute to the development of new anticancer drugs.

4.3.10 MM/GBSA calculation

To further validate the efficacy of the inhibitors against receptor tyrosine kinases (RTKs), the binding free energies were determined using the MM/GBSA method. This was achieved by analysing 100 snapshots collected from the final 20 nanoseconds of the molecular dynamics (MD) simulation trajectories. The results of these calculations are presented in **Table 4.4.**

According to the study findings, the total binding free energy of DPGA and Epirubicin when bound to the FGFR receptor was greater than that of the standard drug, with values

of -47.35 kcal/mol and -49.89 kcal/mol, respectively, while the standard drug exhibited a binding free energy of 46.88 kcal/mol. However, the data presented in **Table 4.4** revealed that Neomycin B did not demonstrate a stronger binding free energy for FGFR compared to the standard drug, with a value of -17.64 kcal/mol, as presented in Table 4.4.

Table 4.4: Free energy analysis of inhibitor complexes with target RTKs protein on the last 20 ns simulation frames.

FGFR				
	ΔG_{bind}	**$\Delta E_{coulomb}$**	**ΔE_{lipo}**	**ΔE_{vdw}**
DPGA	-47.35	-21.04	-12.92	-39.38
Epirubicin	-49.89	-14.05	-15.76	-38.16
Neomycin B	-17.64	-24.57	-4.62	-25.00
Std	-46.88	-20.56	-9.68	-40.32
PDGFR				
	ΔG_{bind}	**$\Delta E_{coulomb}$**	**ΔE_{lipo}**	**ΔE_{vdw}**
Monotropein	-4.80	-5.09	-1.11	-4.12
Epirubicin	-47.88	-10.67	-15.80	-39.96
Neomycin B	-40.74	-29.18	-12.18	-35.99
Std	-42.82	-13.33	-10.78	-41.18
VEGFR				
	ΔG_{bind}	**$\Delta E_{coulomb}$**	**ΔE_{lipo}**	**ΔE_{vdw}**
Naringenin	-39.35	-12.16	-9.60	-30.98
DPGA	-78.37	-18.26	-25.82	-70.29
Epirubicin	-46.21	-9.45	-13.65	-43.35
Std	-50.86	-12.38	-14.27	-46.66

The analysis of the PDGFR receptor unveiled that Epirubicin ligands possess a superior binding affinity towards the PDGFR protein relative to the standard ligand. The binding free energy of Epirubicin and the standard ligand was -47.88 kcal/mol and -42.82 kcal/mol, respectively. The binding free energy of Neomycin B was determined to be comparable to that of the standard ligand, with a value of -40.74 kcal/mol. In contrast, the Monotropein ligand was found to exhibit no significant binding affinity, displaying a very high binding free energy of -4.80 kcal/mol for the PDGFR receptor.

The results of the study showed that among the tested ligands for VEGFR receptors, DPGA exhibited the highest binding affinity and revealed the most favourable total binding free energy value of -78.37 kcal/mol. Meanwhile, the ligand Epirubicin (-46.21 kcal/mol) displayed a similar total binding free affinity to the standard ligand, which showed a value of -50.86 kcal/mol. In contrast, the ligand Naringenin does not demonstrate an improved binding free energy for VEGFR compared to the standard drug, with a value of -39.35 kcal/mol.

By conducting the MM/GBSA analysis, robust data have been obtained that reinforce this confidence in the superior inhibitory potential of DPGA and Epirubicin against FGFR. Additionally, it was found that Epirubicin exhibits more significant inhibitory activity against PDGFR, while DPGA is more effective in inhibiting the VEGFR receptor. These findings suggest that DPGA and Epirubicin may have therapeutic potential as inhibitors of these receptor pathways.

4.3.11 Per-residue decomposition

Furthermore, a per-residue decomposition analysis has been performed to evaluate the role of each amino acid residue in the protein-ligand interactions. Figure 4.14 depicts the per-residue decomposition results for FGFR, PDGFR, and VEGFR.

This analysis provided valuable information on the critical amino acid residues of receptors involved in ligand binding. Based on per-residue decomposition results, it has been observed that amino acid residues displaying binding free energy lower than -1 kcal/mol are vital for maintaining the stability of a complex. Notably, the amino acid residue Ala553, positioned in the hinge region of the FGFR receptor, is essential for binding standard ligands and Epirubicin. Moreover, amino acid residues Leu473, Val481, Ala554, and Leu619 of FGFR have been identified as significant contributors to the binding of Epirubicin and DPGA, along with standard ligands.

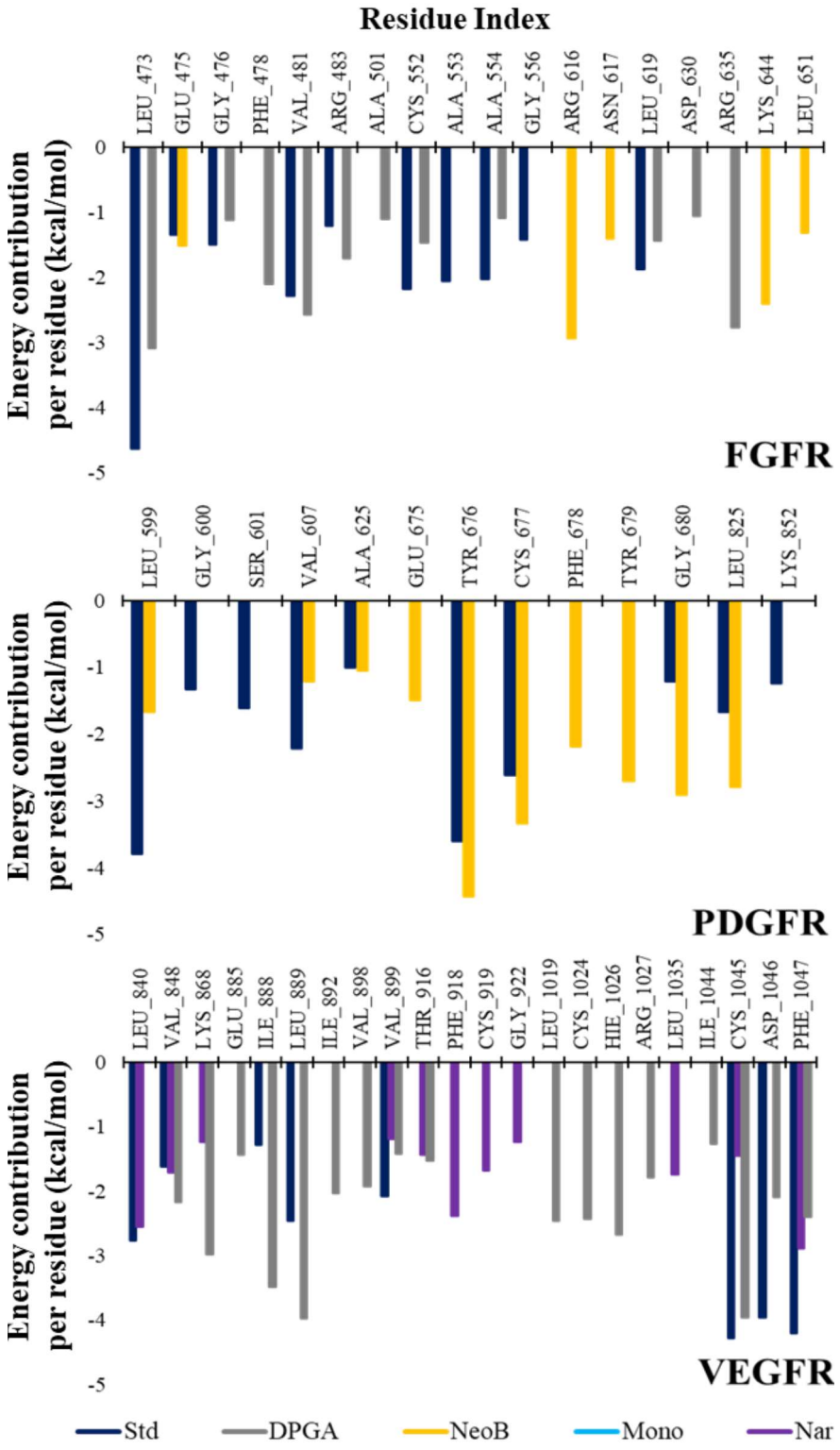

Figure 4.14: Energy decomposition analysis within the protein-ligand complex structure during MD simulation of 200 ns.

The studies have identified that the residues Leu825 in the catalytic loop region and Gly680 in the activation loop region of the PDGFR receptor significantly contribute to

the binding of Epirubicin and Neomycin B ligands, similar to the standard ligand. Furthermore, residues Leu599, Val607, Ala625, Tyr676, and Cys677 also play an essential role in the binding of the standard ligand, Epirubicin, and Neomycin B ligands. These findings provide valuable insights into the molecular mechanisms underlying PDGFR signaling and can aid in developing new therapeutic strategies targeting this receptor.

The amino acid residues Glu885 and Asp1046, present in the DGF motif located in the activation loop of the VEGFR receptor, retain an outstanding effort toward binding with both standard and DPGA ligands, as demonstrated in Figure 4.14**.** Furthermore, Cys1045 and Phe1047, which are close to the DGF motif, are also noted to have an incredible role in interacting with ligand DPGA and Epirubicin, along with standard. Additionally, Isoleucine 888 is also involved in the receptor's ligand-binding mechanism, contributing to the interaction with standard ligand, Epirubicin, and DPGA.

Through the application of computational methods, including molecular docking, molecular dynamics simulation, MM/GBSA calculation, and per-residue decomposition analysis, highly effective secondary metabolites produced by *Streptomyces clavuligerus* have been identified with the potential to inhibit crucial receptor tyrosine kinases associated with cancer. This study revealed the remarkable inhibitory efficacy of compound DPGA and Epirubicin against FGFR and VEGFR receptors. Additionally, Epirubicin exhibited more excellent inhibitory activity against the PDGFR, while DPGA effectively inhibited VEGFR than the FDA-approved drug Pazopanib.

4.4 Conclusions

The objective of this chapter was to explore the potential for cancer therapy using natural sources. This was achieved by assessing the protein kinases inhibitory potential and cytotoxicity activity of the fermented crude extract obtained from *Streptomyces*

clavuligerus. Submerged fermentation was conducted using different media and fermentation conditions. Additionally, the study aimed to identify inhibitors of Receptor Tyrosine Kinases (RTKs) from this strain. DPPH assay depicted a more robust free radical scavenging capacity of *Streptomyces clavuligerus* organic extract (IC_{50} value of 28.90 ± 0.24 µg/mL) with a maximum inhibition percentage of 61±1.04%. In contrast, the aqueous extract exhibited a less potent efficacy, with an IC_{50} value of 74.30 ± 1.13 µg/mL. The presence of protein kinase inhibitors in *Streptomyces clavuligerus* was confirmed through the *Streptomyces 85E* assay or protein kinases inhibitory assay, where a whitish bald or hazy zone, with a diameter of 18 mm, on agar diffusion plates indicated this activity. The cytotoxicity potential of *Streptomyces clavuligerus* organic extracts revealed a potent IC_{50} value of 128.93±3.1 µg/mL against the MCF-7 cell line, compared to SiHa (278.15±4.77 µg/mL), PC-3 (353.14±7.3 µg/mL), and Hop-62 cell lines (464.48±9.2 µg/mL). These findings underscore the promising cytotoxicity potential of the *Streptomyces clavuligerus* extract, particularly against human breast and cervical cancer cell lines.

Furthermore, HR-LCMS analysis identified the various secondary metabolites in both aqueous and organic extracts of *Streptomyces clavuligerus.* In computational analysis, secondary metabolites Epirubicin and DPGA demonstrated inhibitory activity against FGFR. Additionally, Epirubicin displayed a more pronounced inhibitory effect on PDGFR, while DPGA effectively targeted VEGFR. These findings underscore the superior inhibitory potential of Epirubicin against FGFR and PDGFR receptor tyrosine kinases (RTKs).